Remote Sensing of Snow Dynamics over the Vissátvuopmi Palsa Mire, Northern Sweden

Simon Samie

Degree of Bachelor of Science
with a major in Earth Sciences
15 hec

Department of Earth Sciences
University of Gothenburg
2023 B-1266

Faculty of Science

UNIVERSITY OF GOTHENBURG

UNIVERSITY OF GOTHENBURG
Department of Earth Sciences
Geovetarcentrum/Earth Science Centre

Remote Sensing of Snow Dynamics over the Vissátvuopmi Palsa Mire, Northern Sweden

Simon Samie

ISSN 1400-3821

B1266
Bachelor of Science thesis
Göteborg 2023

Mailing address
Geovetarcentrum
S 405 30 Göteborg

Address
Geovetarcentrum
Guldhedsgatan 5A

Telephone
031-786 19 56

Geovetarcentrum
Göteborg University
S-405 30 Göteborg
SWEDEN

Abstract

Palsas are peat hills made of a permafrost core with ice lenses and are very important areas for biodiversity. Today, palsas are also climate indicators for global warming. Due to their sensitive location at the edge of the permafrost zone, they are very vulnerable to a changed climate. Palsas are disappearing faster and faster, as the climate has become increasingly warmer for the past decades. In order to observe these periglacial landforms before they disappear, it is of importance to investigate how a warmer, wetter and more snow-covered climate affects the palsa mires. Above all, snow dynamics is a climate variable that affects the entire permafrost zone. With the help of technological developments, new remote sensing methods have been used in recent decades to map snow dynamics such as snow depth and snow cover, and these can also be applied over palsa mires.

There are yet few studies that use several different types of remote sensing methods to map snow dynamics over the same palsa. Even fewer have combined various remote sensing methods with measurements taken in the field over a palsa mire. The purpose of this study was therefore to investigate how the different remote sensing methods LiDAR (light detection and ranging) and optical satellite data can be used to measure snow dynamics and how their measurements agree to those taken in situ. Weather data was also processed in order to relate climate and topographic parameters with snow distribution over the palsa mire.

Measurements of snow depth and snow cover were performed on two palsa types, a dome-shaped and a ridge-shaped palsa in Vissátvuopmi, Sweden's largest continuous palsa mire. Both UAV (unmanned aerial vehicle) LiDAR and in situ measurements were performed in the field, where Sentinel-2 optical satellite data were collected over the palsas during the time period 2017-2022. Weather data over the study area was also collected and processed.

The results of the snow depth from in situ and LiDAR measurements showed that some measuring points had relatively the same snow depth between the methods, while other points showed greater differences in snow depth between them. A correlation analysis between the different snow depth measurements resulted only in an intermediate correlation of 0.41 for the ridge-shaped palsa and 0.28 for the dome-shaped palsa. The P-values for each correlation was found to be lower than 0.05, indicating that the correlations were statistically significant. The study also shows how much impact meteorological variables such as air temperature and wind have on how snow is distributed over the ridge-shaped and dome-shaped palsas, especially in relation to the palsa's topography. The analysis of Sentinel-2 optical satellite data showed that the ridge-shaped and dome-shaped palsas received an earlier first snowmelt date during the year and a later first snow-free date, which in 2022 resulted in an increase in the snowmelt period by 15 days for the ridge-shaped palsa and 14 days for the dome-shaped palsa since 2019.

Sammanfattning

Palsar är torvkullar som består av en permafrostkärna med islinser och är mycket viktiga områden för biologisk mångfald. Palsar är idag också klimatindikatorer för global uppvärmning. På grund av deras känsliga läge vid permafrostzonens utkant är de mycket mottagliga för klimatförändringar. Eftersom klimatet har blivit allt varmare under de senaste decennierna so har palsområdena krympt i snabbare takt än tidigare. För att observera dessa periglaciala landformer innan de försvinner är det viktigt att undersöka hur ett varmare, blötare och mer snötäckt klimat påverkar palsmyrarna. Framför allt är snödynamik en klimatvariabel som påverkar hela permafrostzonen. Med hjälp av den teknologiska utvecklingen har nya fjärranalysmetoder använts under de senaste decennierna för att kartlägga snödynamik som snödjup och snötäcke, och dessa kan även appliceras över palsmyrar.

Det finns ännu få studier som använder flera olika typer av fjärranalysmetoder för att kartlägga snödynamik över samma typ av pals. Ännu färre har kombinerat olika fjärranalysmetoder med mätningar gjorda i fält över en palsmyr. Syftet med denna studie var därför att undersöka hur de olika fjärranalysmetoderna LiDAR (light detection and rangeing) och optiska satellitdata kan användas för att mäta snödynamik och hur dessa mätningar stämmer överens med de som utförs in situ. Väderdata bearbetades också för att relatera klimat- och topografiska parametrar med snöfördelning över palsmyren.

Mätningar av snödjup och snötäcke utfördes på två palstyper, en kupolpals och en ryggpals i Vissátvuopmi, Sveriges största sammanhängande palsmyrskomplex. Både UAV (unmanned aerial vehicle) LiDAR och in situ-mätningar utfördes i fält, där optiska satellitdata från Sentinel-2 samlades in över palsorna under tidsperioden 2017–2022. Även väderdata över studieområdet samlades in och bearbetades.

Resultaten av snödjupsmätningarna från in situ och LiDAR visade på att några mätpunkter hade relativt samma snödjup mellan metoderna, medan andra punkter visade större skillnader i snödjup mellan dem. En korrelationsanalys mellan snödjupsmätningarna resulterade endast i en medelkorrelation på 0,41 för ryggpalsen och 0,28 för kupolpalsen. P-värdena för varje korrelation visade sig vara lägre än 0,05, vilket tyder på att korrelationerna var statistiskt signifikanta. Studien visar också hur stor påverkan meteorologiska variabler som lufttemperatur och vind har på snöfördelningen över ryggpalsen och kupolpalsen, särskilt i förhållande till palsornas topografi. Analysen av optiska satellitdata från Sentinel-2 visade att ryggpalsen och kupolpalsen fått ett mer tidigt första snösmältningsdatum under året och ett senare första snöfritt datum, vilket år 2022 resulterat i en ökning av snösmältningsperioden med 15 dagar för ryggpalsen och 14 dagar för kupolpalsen sedan 2019.

Acknowledgements

I would like to take this opportunity to thank everyone who helped me through this project and made it possible. First, I would like to thank my supervisor, Associate Professor Heather Reese for all the support and guidance as well as providing data throughout the project and for allowing me to join the field trip to Saarikoski. I would also like to thank PhD student Cas Renette for his help with materials, data process and tools during the field studies and for all the advice and feedback during the work. I also want to thank my fellow student Calle Åquist-Holm for the good cooperation and feedback we have been able to contribute to each other. Thanks also to course leader Mark Johnson and to my classmates for constructive support and advice during peer-reviewing. Finally, a special thanks to Leif Vilhelmsson for housing and scooter support during the field study in Saarikoski.

List of abbreviations

DTM	Digital Terrain Model
DOY	Days of the Year
GIS	Geographical Information System
GPS	Global Positioning System
LiDAR	Light Detection and Ranging
MSI	Multi-Spectral Instrument
R	Correlation Coefficient
R^2	Coefficient of Determination
RMSE	Root Mean Square Error
RTK	Real Time Kinematic
UAV	Unmanned Aerial Vehicle

Table of Contents

1. Introduction

Palsas are peat hills consisting of peat mounds with a perennial core of ice and frozen peat and often also mineral soil (Zuidhoff, 2003). They are one of the most characteristic periglacial landforms of the permafrost landscape (Hjort, 2006) and occur within the southern limits of the permafrost zone, within Europe only in northern Scandinavia (Zuidhoff & Kolstrup, 2000). Palsa mires are a distinctive wetland type and according to the EU's habitat directive, are a priority nature type. Palsas are counted as some of the most threatened nature types within the EU and needs to be protected, since they are very non-resistant to changes in climate (Länsstyrelsen, 2014).

Palsas vary both in shape, size and height depending on their development and the influence of various climatological and topographical factors that affect the palsas' growth, with some palsas being as high as 12 m and ranging between 2 m to 150 m in diameter (Kujala et al., 2008; Seppälä, 2006). Geomorphologically, they are characterized as having steep slopes, rising above the mire surface (Figure 1) which contribute to large amounts of snow accumulating around them (Kujala et al., 2008). Palsa mires are also important habitats as their heterogeneous characteristics make them, from an ecosystem perspective, environments of high biodiversity but also of cultural importance such as palsa mires being a rich source of reindeer pastures and ideal land for berry picking (Verdonen et al., 2023).

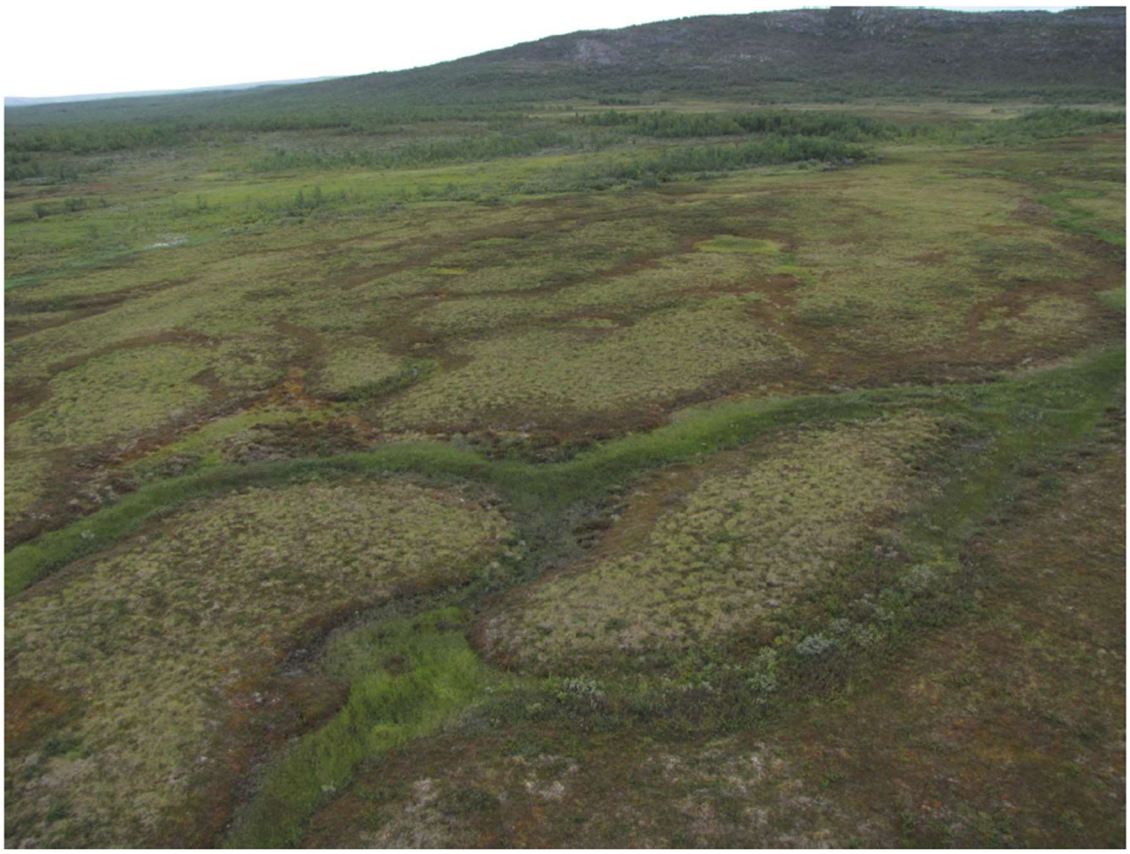

Figure 1. Lowland palsa mires in Vissátvuopmi, Sweden's largest palsa mire complex. Image taken in 2014. Photo: Susanne Backe, Länsstyrelsen Norrbotten.

Since palsas have a distribution at the outer limit of the permafrost zone, they are very sensitive to variations in the climate (Olvmo et al., 2020) and several recent studies (Borge et al., 2017; de la Barreda-Bautista et al., 2022; Olvmo et al., 2020) have shown that these unique landforms are declining at an increasingly rapid rate in the last decades due to climate change. Palsas are generally associated with the natural limitation of what permafrost can withstand against changes in climate, as palsas usually require an annual average air temperature lower than 0°C, usually a few degrees below freezing (Seppälä, 2017).

With the climate changes of recent decades, more and more studies have investigated which meteorological parameters play the greatest role in contributing to the palsa degradation of recent years. Two parameters that affect palsa degeneration the most are air temperature and snow depth (Sannel et al., 2016) since both these parameters control ground temperature, which contributes to much of the permafrost beginning to thaw (Sannel, 2020). In previous studies of palsas, snow dynamics such as snow depth and snow cover have been of interest to map over the palsas since climate change has led to increased temperatures and precipitation in the subarctic region, which contribute to thicker layers of snow over the palsa mires (Verdonen et al., 2023). A deeper snow depth over the palsas has shown to increase the soil temperature underneath, providing conditions that cause the permafrost inside the palsa to thaw more quickly. In addition, it is known that wind has a large influence on the distribution of snow over the palsa, but it is still relatively unstudied (Seppälä, 2017).

According to Kinar and Pomeroy (2015), some of the various methods to observe snow dynamics is traditional in situ observations, non-destructive lidar and radar methods and satellite remote sensing. The development of remote sensing provides helpfull tools to understand and evaluate many of these dynamics connected to surface interpretations and changes in land cover identical with permafrost degradation over broad regions (Runge & Grosse, 2019). Since its launch in 2017, Sentinel-2 has been able to take even sharper images of remote areas on Earth in even higher resolution than its predecessor Landsat (Gascoin et al., 2019). Drone-based platforms, also known as UAV (unmanned aerial vehicle) equipped with LiDAR (light detection and ranging) are another, new remote sensing method that has expanded greatly and is expecting to revolutionize the use of remote sensing in natural sciences (Proulx et al., 2022; Sankey et al., 2017). Because UAV LiDAR is such a new technology, there are few studies that have investigated how it can be used to map snow dynamics over permafrost features such as palsa mires.

1.1 Purpose and research questions

The aim of this thesis is to investigate how the snow distribution is over two specific palsa forms, a dome-shaped palsa and a ridge-shaped palsa in the Vissátvuopmi palsa mire complex in northern Sweden. This is done by using in situ and UAV LiDAR data measured over the ridge and dome palsas in 2023 and relate these dynamics to topographic and climate parameters, as well as optical remote sensing data between the years 2017 to 2022. The questions to be answered based on this aim are as follows:

1) How well does UAV LiDAR data agree with in situ snow depth data collected over the ridge-shaped palsa and the dome-shaped palsa?

2) How does the topography and weather parameters affect the snow over the ridge-shaped and dome-shaped palsas, and how do the snow dynamics compare over the palsas?

3) Is it achievable, with the help of weather data and optical satellite data, to find an exact time period over the years 2017-2022 when the snow over the ridge-shaped and dome-shaped palsas is starting to melt and when the palsas become snow-free?

Expectations of the study are that it should be able to contribute to an increased understanding of the accuracy of the UAV LiDAR to measure snow depth and to determine the influence of topography, climate and geomorphology of the palsas on snow. The hope is that the study can be used to develop and improve future studies that will investigate the impact of snow dynamics on palsa degradation.

1.2 Background

1.2.1 Palsa and permafrost

The word palsa is originally a Sami word and literally means "a rise in a bog". Palsas are a unique morphological landform, and have a particular biological diversity, with a which are sensitive ecosystem and outstanding locations for vegetation, hydrology, carbon cycle and wildlife. (Seppälä, 2017). Depending on the morphology of the pals, they are classified into several types. Some palsa types are elongated, string-shaped, longitudinal, ridge-shaped, dome-shaped and plateau-shaped. A larger accumulation of palsas is usually referred to as a palsa mire (Seppälä, 2006).

Palsas are a great source of carbon stores on Earth thanks to the fact that they are frozen all year round. Due to a changing climate and global warming, many permafrost landforms are beginning to release carbon into the atmosphere as a result of their thawing (Seppälä, 2017; Zuidhoff & Kolstrup, 2000). Permafrost can only be found within the palsa and not on it, making up the palsa's frozen core (Kujala et al., 2008).

1.2.2 Palsa degradation

Permafrost and palsa degradation are characterized by warming ground temperature, spread of thermokarsts (Figure 2) and an increased active layer thickness (ALT), which occurs throughout the permafrost area in the northern hemisphere, but also in remote mountain environments where partial permafrost degradation occurs (Verdonen et al., 2023). Thermokarsts are small lakes formed as a result of ground collapse due to thawing of the ice-rich soil (Sannel et al., 2016). The ALT is the layer above the permafrost that thaws in late spring and summer and then freezes again in winter (Seppälä, 2003). Due to global climate warming, losses of large contiguous permafrost areas are expected to become a reality soon. A changed climate, especially in the subarctic permafrost areas, is expected to contribute to increased precipitation, which means an increased snow cover that is harmful to the permafrost landscape (Borge et al., 2017).

Since the 1950s, palsas have shown a degeneration, which has contributed to the collapse of many old and characteristic palsa mires as a result of a changed climate in the permafrost region (Zuidhoff & Kolstrup, 2000). The palsa area has been disappearing at an increasingly rapid rate, and according to Borge et al. (2017), aerial photographs of observed thermokarst lakes have existed for several decades, indicating that the palsa degeneration has been ongoing for a long time. A thermokarst lake forms when a palsa's frozen core thaws, resulting

in a lake in the form of a pond. Thermokarst lakes become more common in the permaforest zone as the palsa landscape begins to thaw (Seppälä, 2006).

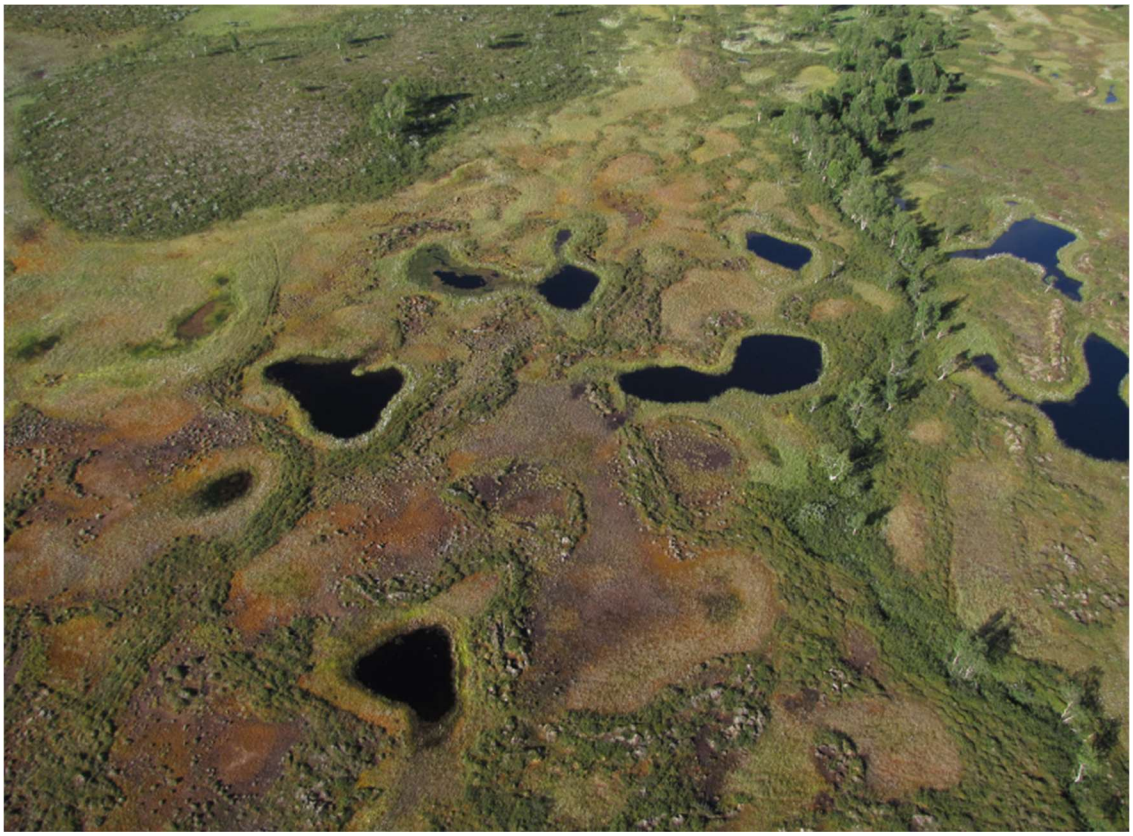

Figure 2. Picture taken 2012 over the palsa mire Laivadalen in northern Sweden. Collapsed palsas have contributed to the thermokarst lakes around the palsa mire. Photo: Susanne Backe, Länsstyrelsen Norrbotten.

1.2.3 Snow dynamics

Snow covers up to 40-50 % of the northern hemisphere's land cover mass and 44 % of the Earth's land mass in total during wintertime and is of essential influence for the climate (Dietz et al., 2011; Dumont & Gascoin, 2016). Snow dynamics is a collective name for different types of snow parameters, i.e., different conditions of snow, such as snow depth, snow cover, snow melting, etc. (Keyser et al., 2022). For understanding the Earth's climate system, snow dynamics are crucial to comprehend, since snow processes are main components in the hydrological cycle in snow rich regions (Hori et al., 2017; Kopp et al., 2019).

Reliable information on snow dynamics such as snow depth and snow cover are not only important for assessing water resource availability for snow-rich areas, but also provides vital indicators essential for investigating the impact of climate change (Kopp et al., 2019). Investigate snowpack density and water stored in the snowpack, known as snow water equivalent (SWE) are some of the important reasons for being able to map snow (King et al., 2023).

Ever since the beginning of the 20th century, there has been an increase in air temperature and precipitation in the high northern latitudes, which in the northern hemisphere can result in an increase of snow and has a huge impact on the palsas due to its low thermal conductivity

(Sannel et al., 2016). An increasing air temperature in combination of a thick snow layer on top of a palsa may result in the soil underneath becoming more insulated and receiving increased moisture (Figure 3), causing the soil to reduce its heat fluxes (Olvmo et al., 2020; Sannel, 2020). A continuous thick layer of snow over the palsas may eventually result in block erosion in the palsa (Olvmo et al., 2020).

Figure 3. Photo taken on top of a dome-shaped palsa in Vissátvuopmi, April 2023. The topography of the palsa is decisive for how the snow is distributed over the palsa, with a generally snow-free top and snow accumulations around the edges.

1.3 Study area

The study area is located in the palsa mire complex called Vissátvuopmi, around N 68°74'50", E 21°11'30" (Olvmo et al., 2020) and approximately 1.6 km southwest of the settlement of Saarikoski at the border between the northernmost Sweden and Finland (Figure 4). Vissátvuopmi is in the Arctic region and the distance to the nearest coastline, located in Norway, is approximately 73.3 km NW. Vissátvuopmi consist of the largest contiguous area of palsa bogs in Sweden, holds an immense 273 hectares of palsa, which in 2014 constituted 13.8% of Sweden's palsa area (Länsstyrelsen, 2014). The study area was visited during the 17th to 22nd of April 2023 for data collection over the ridge-shaped and dome-shaped palsas.

1.3.1 Ridge-shaped palsa and dome-shaped palsa

The ridge-shaped and dome-shaped palsas in the mire complex are located approximately 1.1 kilometers apart, where the ridge-shaped palsa is in the northwest part of Vissátvuopmi and the dome-shaped palsa located in the southeast. The ridge-shaped and dome-shaped palsas

stand out because they are taller (3-4 m) compared to the surrounding palsas in the complex (Olvmo et al., 2020).

1.3.2 Climate and topography

According to Sveriges Meteorologiska och Hydrologiska Institut (SMHI), Vissátvuopmi falls under the ET category according to the Köppen climate system, which is classified as polar and tundra climate (SMHI, 2022a). The annual mean temperature for the normal period 1991-2020 in the area lies between -1 to -2º C (SMHI, 2022b).

Most of the study area in Vissátvuopmi is within a valley about 450 meters above sea level (m a.s.l.) surrounded by mountains and lakes. The mountain closes to the palsa mire complex are approximately 500 m a.s.l. North of Vissátvuopmi the lake Veivijärvi is located, where the ridge-shaped palsa is located just southeast of the lake. Another lake, Vittankijärvi is in the south with the dome-shaped palsa located just at the north tip of the lake. Apart from the previously mentioned different palsa forms, the topography around the area is relatively flat, with some of the tallest palsas, such as the ridge-shaped and dome shaped palsas, rising 3-4 m above the ground, with thermokarst lakes being present around the palsa domiain. Low-shrubs, mosses and lichens are the dominant vegetation type and the absence of taller vegetation such as trees is prominent for the palsa mire (Olvmo et al., 2020).

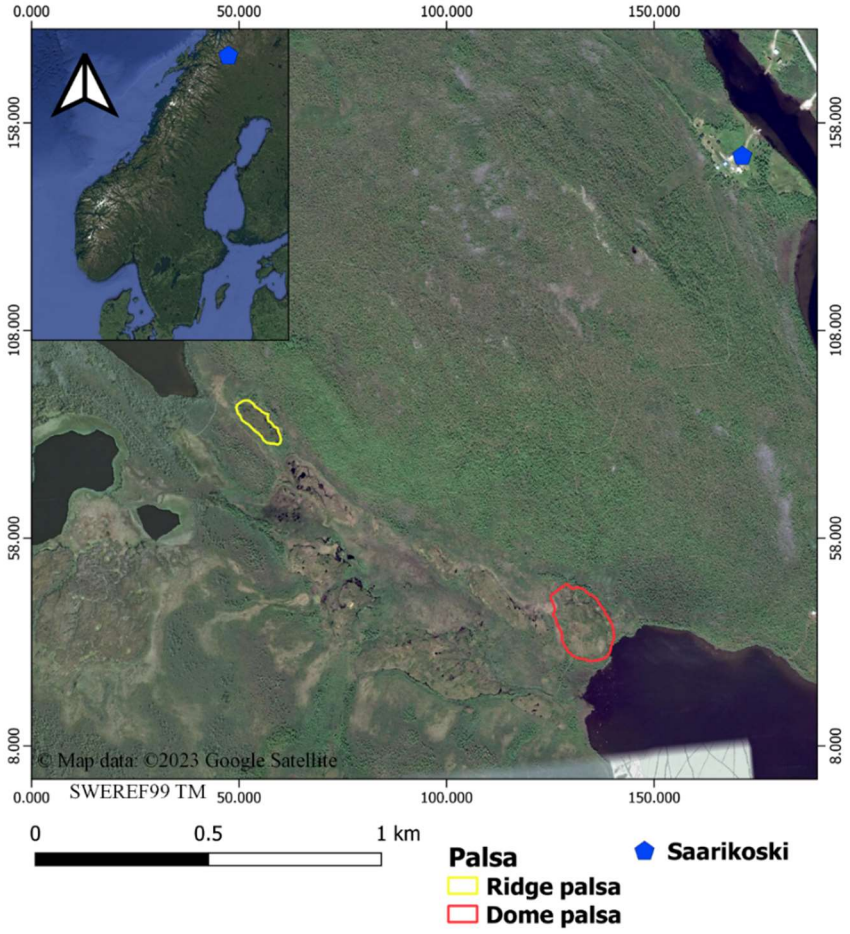

Figure 4. The study area of Vissátvuopmi and the settlement of Saarikoski's location in northern Sweden. The ridge and dome palsas where the snow depth measurements were taken is presented in yellow (ridge-shaped) and red (dome-shaped).

2. Materials and methods

In order to map snow dynamics over the ridge-shaped and dome-shaped palsas in this study, field measurements were carried out in Vissátvuopmi palsa mire between 18-19 April 2023. The measurements performed were manual snow depth measurements and UAV LiDAR scanning over the ridge-shaped and dome-shaped palsas. Orthophotos were also taken over the ridge and dome palsas to estimate the snow cover and topography over both palsas. The snow depth measurements and orthophotos were then processed in GIS-program for visualization of snow depths over the two palsas.

The survey of snow cover and snowmelt was conducted with optical satellite images taken with Sentinel-2. Since the Sentinel-2 data was only available first in 2017 and forward and the year 2023 does not have fully updated satellite and weather data, the study period for weather data and optical satellite data over Vissátvuopmi was limited for the years 2017 to 2022. Meteorological weather data, air temperature and wind direction were also analysed, to understand during which period of the year the snowmelt occurs and how the snow is distributed over the ridge-shaped and dome-shaped palsas.

2.1 Remote sensing tools

With the help of UAV, mostly referring to as drones, new possibilities to map ground and snow features have developed, such as UAV carrying LiDAR, orthophoto images and photogrammetry (Žabota et al., 2023). UAV platforms have contributed with unique opportunities to take images with a low cost and still provide good temporal and spatial resolutions as a result. UAV platforms are also popular due to their flexibility to capture images at both regional and local scales. Another major advantage of the flexibility of UAV platforms is that they can avoid certain obstacles that other remote sensing platforms struggle with, such as satellite return times, flight coordination, cloud cover, and other similar atmospheric influences on imagery (Sankey et al., 2017).

LiDAR are an active remote sensing method that use light pulses to measure and acquire high resolution point clouds and is not affected by different kinds of weather disturbances such as cloud coverage or windy conditions (King et al., 2023). When LiDAR sends out a light pulse, it measures the travel time of each pulse that is transmitted back to the sensor, which helps LiDAR measurements quickly estimate the elevation of a target (Feng et al., 2023).

The LiDAR data for ground and elevation scanning were acquired from a DJI (Da Jiang Innovations) matric 300, which carried a YellowScan Mapper+ LiDAR scanner (Figure 5), flying at 35 m flying height. The data were processed into a DTM (digital terrain model) using YellowScan Cloud Station software. The DJI Matrice 300 drone is equipped with a RTK (real time kinematic) receiver that collects data from satellites while flying, which gives the measurement points taken by LiDAR to have a more accurate precision than regular GPS global positioning system). The yellow scan mapper itself is a high-performance laser scanner. LiDAR's used in collecting the elevation data the 18th of April 2023 had a precision of 2 cm. The orthophotos were acquired from a DJI Phantom 4 drone with a RGB camera, at a flying height of 20 m. Two snow-on orthophotos was taken, one over the ridge-shaped palsa on 18th of April, and one over the dome-shaped palsa on 20th of April 2023. In the orthophoto of the snow-covered dome-shaped palsa, there are some areas from the middle of the palsa that are missing from the orthophoto, due to lack of stereo photo coverage. The orthophoto was created using Agisoft Metashape software and has a pixel size of 1.679e-07 x 6.079e-08 cm. Two orthophotos from a snow-off period in August 2021 were also added to the project

for topographic comparison of the snow-on orthophotos. All the orthophotos in this study were provided by Heather Reese.

Figure 5. The DJI Matrice 300 drone carrying the YellowScan Mapper+ LiDAR scanner.

The use of optical satellites for mapping very large areas at a very distant places on the Earth, is an advantage for areas that is hard to reach by land (Winsvold et al., 2016). Since 2015 and 2017, the European Space Agency (ESA) has launched two identical optical satellite sensors called Sentinel-2A (2015) and Sentinel-2B (2017). A technological feature of Sentinel-2A and 2B is that they have the Multi-Spectral Instrument (MSI) aboard, and the MSI is also a multi-spectral imager, orbiting at an altitude of 786-km (Runge & Grosse, 2019). The MSI's 13 spectral bands give multispectral imagery at different spatial resolutions of 10 m, 20 m and 60 m (Runge & Grosse, 2019). Both 2A and 2B operate together to achieve frequent revisits and high availability of images of the Earth's surface. Sentinel-2A and 2B have an equatorial revisit time period of 10 days but as they operate together, the joint revisit period of only 5 days over the equator (Aalstad, 2019; Runge & Grosse, 2019). In polar regions, the revisit period is noticeably shorter, 1-2 days, due to the orbits assemble (Aalstad, 2019). For acquire snow cover over time and find the first snowmelt and snow-free dates over the ridge-shaped and dome-shaped palsas between 2017-2022, Sentinel-2 optical images were observed and downloaded from the Sentinel Hub EO Browser (Browser, "n.d.") and Copernicus Open Access Hub (Hub, 2023), both powered by ESA.

2.2 Tools for in situ measurements

For the snow depth measurements in situ over the ridge-shaped and dome-shaped palsas, a measuring stick with the measurements of 0-120 cm was used for measuring snow depth. An Emlid Reach RS2 RTK-GPS unit with 2 cm precision in good conditions, was intended to be used for positioning measurements, using a base station and a rower measuring every point taken. Due to short battery life of the Emlid Reach RS2, the decision was made to use the smartphone application Qfiled (Qfield, 2023) instead. Qfield is a Qgis based app for fieldwork and the GIS analysis was also performed in Qgis. The Qfield app was based on the GPS-precision in the same smartphone used, which had an accuracy of around 4-9 m (Korpilo et al., 2017).

2.3 Snow depth measurements

The field-based snow depth measurements were carried out in Vissátvuopmi during the 18th to 19th of April 2023. As the snow cover over the ridge-shaped and dome-shaped palsas made it difficult to determine where the boundaries across the both palsas was, LiDAR generated DTMs of the palsas taken the 4th of September 2022 over the ridge-shaped and dome-shaped

palsa were added to Qfield (Figure 6). The DTMs were used as help in deciding where the snow depth above the ridge-shaped and dome-shaped palsas should be taken. All the snow depth measurements were measured in centimeters.

2.3.1 Dome-shaped palsa

The snow depth measurements over the dome-shaped palsa (Figure 6a) were taken in the afternoon the 18th of April. The measurements of the snow depth first began at the north-western part of the dome-shaped palsa, with a planned method of measuring in north-south transects with about 5 meters distance between each measurement. As there were difficulties in following straight transects across the dome-shaped palsa, partly due to its topography, it was decided that measurements over the entire palsa should be carried out without necessarily being straight transect lines. Depending on the topography, an approximate distance of 4-5 m between the snow depth measurements was followed.

For each snow depth measurement, the measuring stick was inserted into the snow until it hit the ground. The snow depth was then recorded based on the stick for each measuring point. To be sure that the probe went down far enough and just hit the ground under the snow, a couple of control measurements were taken in places with great topographical variation on the palsa, using the coarser and thicker probe in the snow to estimate where the ground surface under the snow was. A point for every snow depth measurement was added in the Qfield LiDAR map over the palsa. A total of 79 snow depth measurements were carried out over the dome-shaped palsa.

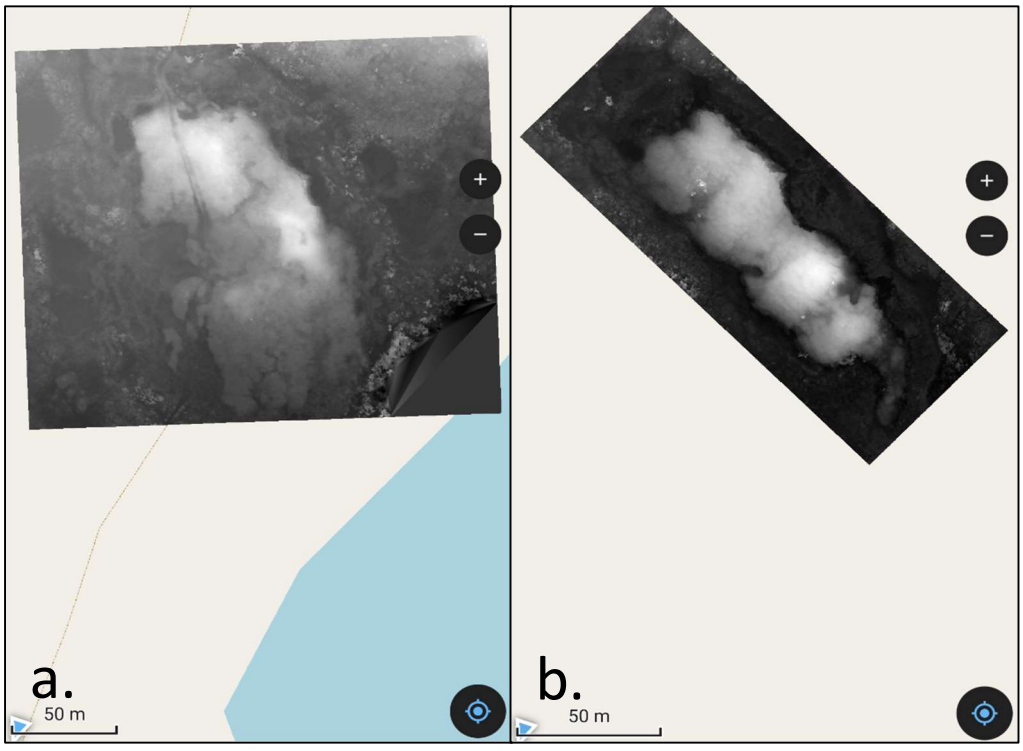

Figure 6. LiDAR generated DTMs in Qfield over the dome-shaped (a) and ridge-shaped (b) palsas that were used for following palsa boundaries and set measurement points. The maps were using SWEREF99TM.

2.3.2 Ridge-shaped palsa

Snow depth measurements over the ridge-shaped palsa were carried out on the day of 19th April. The LiDAR DTM of the ridge-shaped palsa (Figure 6b) was used in Qfield to delineate where the border of the ridge-shaped palsa under the snow was. The same distance of 5 m between the snow depth measurements was used as for the dome-shaped palsa. The same tools, measurement stick for the snow dept taken to the bare ground and the coarse stick for control depth points were used the same way as when measuring the dome-shaped palsa. A total of 91 snow depth measurements were taken over the ridge-shaped palsa.

2.4 GIS analysis of snow depth

The snow depth measurements were converted into a shapefile format for processing in GIS. These was provided and added into the GIS analysis. The LiDAR data consisted of two snow-on elevation data layers collected on 18th April 2023, one for the ridge-shaped and one for the dome-shaped palsas. Two LiDAR data digital elevation model (DTM) layers taken 4th September 2022 on a snow-free period over the same dome-shaped and ridge-shaped palsas was used for calculating the LiDAR snow depth. The reference system SWEREF99TM was used for all mapping. Both LiDAR layers were collected with a precision of 2 cm.

To calculate the LiDAR snow depth, the snow-free DTM model layers from September 2022 were subtracted from the snow-covered elevation model from April 2023, so that the snow depth in the layers only remains. To be able to compare the measurements taken in situ with snow depth layers from the LiDAR, the tool “Sample Raster Values” was used to sample the raster values from the LiDAR snow depth layer to point values where the same snow points were taken in situ. For the dome-shaped palsa, four of the northernmost in situ measurements had to be left out, since LiDAR data did not cover these points.

The two snow-on orthophotos taken over the ridge-shaped palsa on 18th April 2023 and the dome-shaped palsa on 20th April the same year, were also provided and compared with other two snow-off orthophotos from August 2021 taken on each palsa. The orthophotos were important for understanding how the snow depth over the ridge and dome palsas looks, how it is distributed over the two palsas and how the terrain can be compared to the snow depth measurements.

2.5 Data analysis

After all the snow depth values from the LiDAR calculations and in situ were compiled, scatter plots were made, one for the ridge-shaped and for the dome-shaped palsas separately. A scatter plot for the daily mean air temperature for Naimakka-Kilpisjärvi and daily mean from Saarikoski were also made. A linear regression was performed between snow depth measurements in situ and snow depth measurements for LiDAR (Eq 1).

$$y = a + bx \quad (1)$$

where y was the (in situ) snow depth measurement and x was the (LiDAR) measured snow depth. The constant a is the intercept and b the slope (Asuero et al., 2007). By determining the linear regression for each plot by Eq 1, the Pearson’s correlation coefficient was also calculated. A correlation represents the direction and strength of a relationship between two variables (Asuero et al., 2007). To determine how the correlation between the in situ and LiDAR measurements relate to each other, the square of the correlation coefficient (R^2) was calculated for each plot. The R^2 takes values between 1 and -1, where 1 means there is a

strong positive relationship between the variables and -1 means there is a strong negative relationship between the variables. A correlation of 0 means there is no relationship. A p-value for comparing if there is statistical significance between both variables where also calculated. If the p-value < 0.05, there will be a significant relationship between the variables. If the p-value > 0, there is no significant relationship between the variables. Another valuable statistic measurement is the standard deviation (Std) which shows the average amount of variability in a dataset. By determining the Std, it can tell how far each value lies from the average mean in a dataset and is always positive (Asuero et al., 2007).

To investigate how possible errors in the dataset could be compared to the actual value, the root mean square error (RMSE) of the snow depth measurements over the ridge-shaped and dome-shaped palsas was calculated. The RMSE measures the average difference between values predicted by a model and the actual values (Asuero et al., 2007; Proulx et al., 2022). It is used to measure the difference between the estimated values by a model and the actual values observed (Eq 2).

$$RMSE = \sqrt{\frac{\Sigma(y_i - y_p)^2}{N}} \quad (2)$$

where y_i is the actual values, y_p the predicted values and N the number of observations/data points. A low RMSE value close to 0 indicates that the estimated and observed data are close to each other, showing a better accuracy.

For daily air temperature, a regression and correlation analysis were performed between air temperature from Saarikoski station and calculated daily air temperature between Naimakka and Kilpisjärvi. Since the weather data from GU's station in Saarikoski was only used on 6 September 2022, the calculated daily mean air temperature from Naimakka-Kilpisjärvi was also used from 2022-09-06 to 2023-04-22.

2.6 Weather data analysis

In order to understand what time of the year the snowmelt begins over Vissátvuopmi, weather data were needed to determine when the first snowmelt over the palsa mires occurs. Snowmelt is forced by the weather, with air temperature being the most fundamental parameter. Wind data was also of interest to investigate how mainly the wind direction over the ridge-shaped and dome-shaped palsas affects the amount and distribution of snow cover and snow depth on top and around the ridge-shaped and dome-shaped palsas. The temperature and wind data from Naimakka was downloaded from the Swedish Meteorological and Hydrological Institute (SMHI, "n.d.") and could only be downloaded over the years 1995-2023. Temperature data from Kilpisjärvi was downloaded from the Finnish Meteorological Institute (FMI, "n.d.") for the years 2017-2022. Weather data from a local Saarikoski weather station set by the University of Gothenburg (GU) was collected the 22nd of April 2023, and provided temperature data for the period 6th September 2022 to 22nd of April 2023.

As GU's weather station was only put into use on 6th September 2022 and has not been collected or analyzed before, it is unknown how the weather data from this station compares to other adjacent weather stations. It was therefore considered interesting to investigate how well the air temperature data from GU's weather station correlates and compare with the mean value of air temperature between Naimakka and Kilpisjärvi weather stations.

2.6.1 Air temperature

Because no historical temperature data record exists over the Saarikoski area, temperature records from the nearby Swedish weather station in Naimakka, 18 km south and the nearby Finnish weather station in Kilpisjärvi, 33 km north, had to be downloaded and processed to find a mean temperature between Naimakka and Kilpisjärvi, which would represent an average close to the temperature found in Saarikoski. The original data from SMHI and FMI both contained daily temperature means. From the SMHI data the years 2017-2022 were extracted. When the dataset was examined for any errors or missing values, it was discovered that in the Naimakka dataset between 2019-05-20 and 2019-06-18, one month of temperature values were missing. Linear interpolation was used to replace values for the first half of the missing month using data from April and the other half of the missing month using data from July of the same year.

To obtain daily average values over the Saarikoski area, the average values of the data from Kilpisjärvi and Naimakka were calculated and a new dataset for the Saarikoski daily means were created. After the daily average temperature was calculated, the temperature data from the Saarikoski weather station (Figure 7) located around 250 m southeast of the settlement was linked with the new daily mean dataset to compare how well the two datasets agreed. The data from Saarikoski station contained temperature values back to 6th September 2022.The new combined temperature was then plotted to get an overview of the Saarikoski daily mean for the period 1 January 2017 to 22 April 2023.

Figure 7. The Saarikoski weather station set up by University of Gothenburg.

To find which time of the year the snow started to melt, an average monthly climatology over the years 2017-2022 was created. Climatological averages are based on the mean of a climate

variable value over a specific time period (Copernicus, 2020) and was used to investigate during which months of the year the temperature begins to exceed 0 º C. For the months that were within the snowmelt period, an annual average temperature was taken for each month between 2017-2022.

2.6.2 Wind

Since SMHI's weather station at Naimakka were considered to be the weather station with the most identical topography to that at Vissátvuopmi, it was decided that wind data should be downloaded from there. Just as with the air temperature data, the wind data ranged over the years 2017-2022 and were examined for possible errors or missing values. Since the wind data was coming from the same original dataset from Naimakka, a monthly dataset of values between 18-05-2019 to 18-06-2019 was missing, together with one missing value in 2018-09-02. As with the Naimakka air temperature, all the missing values were interpolated to new mean values. As the wind data contained hourly values, they were converted to daily values to be easier to process and visualize in a wind rose plot.

2.7 Optical satellite data analysis

The criteria for determining what counts as the first melting of snow over a palsa was based on literature from Kujala et al. (2008) and Seppälä (2017) describing snow as thickest around the lower edges of the palsa and studies made by Sannel (2020) described how the average snow depth between December and April on peat plateaus and palsas is lowest in the central parts and furthest along the edges of a raised peat plateau. After April, air temperature and wind have an increasingly strong influence on the snow distribution and snowmelt over the palsas, which means that the snowmelt on the summit usually does not regain a thicker snow cover after this period. (Sannel, 2020; Seppälä, 2017). Based on the previous studies and literature, the definition of first snowmelt was established as when the first peak of the ridge-shaped and dome-shaped palsa is visible on the satellite images. For the ridge-shaped and dome-shaped palsas to be counted as completely snow-free, no snow had to be present in the images on top of the two palsas.

To understand the length of the snowmelt period over the ridge-shaped and dome-shaped palsas, the date of the first snowmelt over the ridge-shaped and dome-shaped palsas as well as the date when the palsas could be estimated as completely snow-free, were determined using optical satellite images. It was also important to examine the snowmelt period between the ridge-shaped and dome-shaped palsas, since they differ topographically, with the ridge-shaped palsa being higher and narrower and the dome-shaped palsa lower and wider. The optical satellite data for the snow cover over the ridge-shaped and dome-shaped palsas was examined and downloaded from Sentinel Hub EO Browser as images, based on the result from the monthly climatology where the period April-June could be read as the time over the years when the first snowmelt over Vissátvuopmi should occur.

For each year between 2017-2022, two dates on the ridge-shaped palsa and two on the dome-shaped palsa were taken. One date for the first snowmelt and one date when the palsa could be assumed to be completely snow-free. All cloud-free images were examined from the beginning of April to the end of June for each year between 2017-2022. This is to rule out earlier snowmelts weeks before the first observed snowmelt date, or late snow cover after the first observed snow-free date. The dates were then plotted in a line graph where days of the year (DOY) were used to more easily compare the snowmelt period between the ridge-shaped

and dome-shaped palsas. Two of the examined dates, first snowmelt date 2022-04-20 and first snow-free date 2017-06-09 was downloaded as JPG-files from Copernicus Open Access Hub for better visualization of a first snowmelt and snow-free date over the ridge-shaped and dome-shaped palsas. A third date, 2022-04-09 was downloaded and presented to get a better overview of the progress of snowmelt over the two palsas.

A recurring problem with finding an exact date for when the snowmelt starts and ends is that many times the optical satellite images are obscured by clouds, which means that on some dates only an estimate of the first snowmelt and snow-free date can be made. For other years, a clearer difference and exact date could be extracted from the satellite images. Due to cloud coverage, a week before the first observed snowmelt and a week after the first observed snow-free dates were always examined to ensure that no snowmelt or new snow had fallen over the two palsas.

3. Results

The section presents the results for the snow depth measurements, weather data analysis and optical satellite images for snow cover. The snow depth measurements are presented in maps together with the remote sensing analysis.

3.1 Snow depth and remote sensing

In Figure 8, the snow depth measurements performed in situ were compared with the LiDAR measurements of snow depth. The LiDAR layer is based on the snow depth difference between the snow-off elevation layers in Figure 9 and Figure 11 and the snow-on elevation layers in Figure 9 and Figure 11.

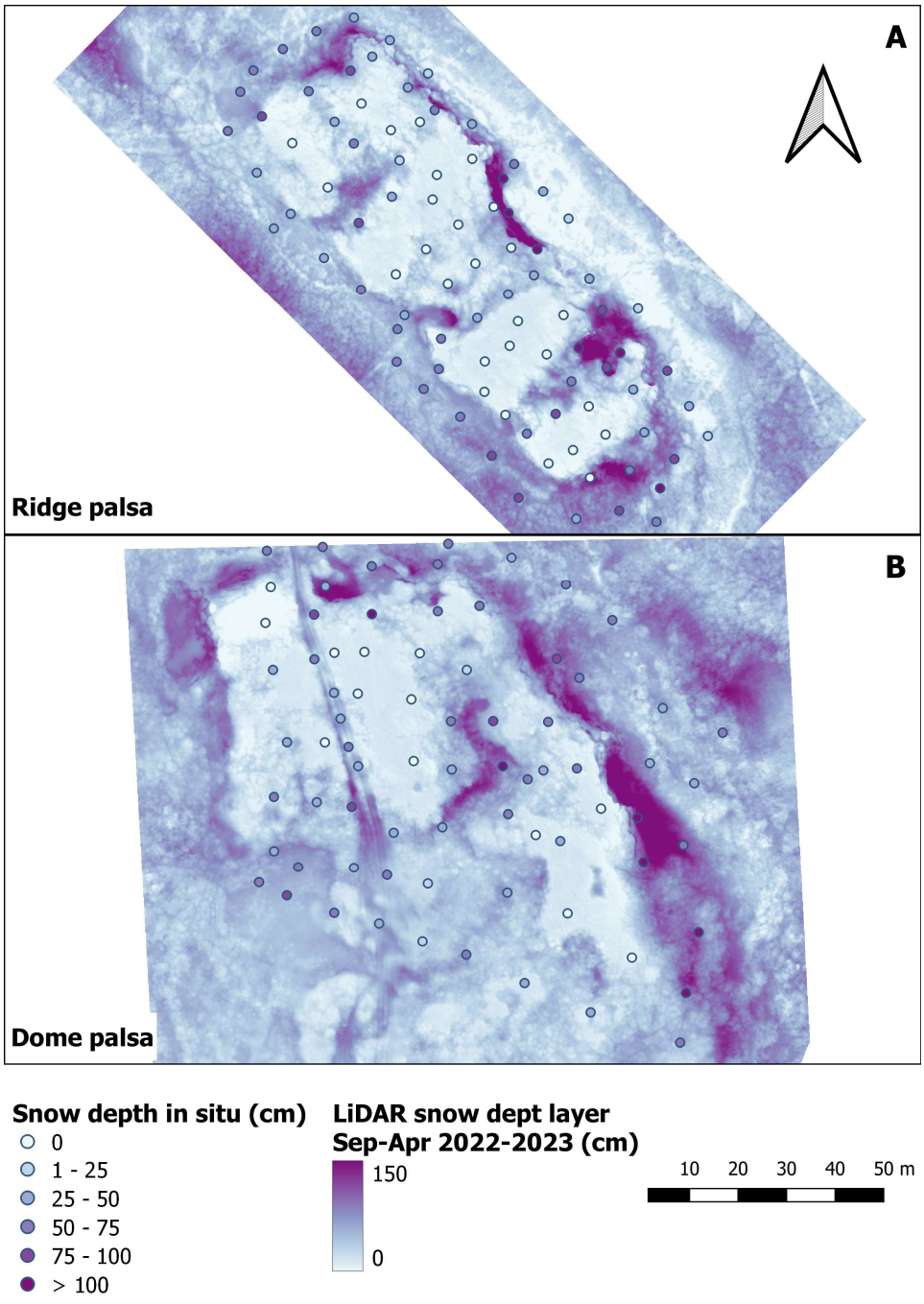

Figure 8. Snow depth points in situ compared to LiDAR-measured snow depth over the ridge-shaped palsa (A) and the dome-shaped palsa (B).

Figure 9 shows the difference between snow depth measurements in situ (Figure 9A & B) and snow depth calculated from LiDAR data (Figure 9C & D) between snow-on (Figure 9A & C) and snow-off height data (Figure 9B & D). On the northwest elevation line of the ridge-shaped palsa, there is an agreement between snow depth measured in situ and LiDAR-measured snow depth. The high correspondence in snow depth measurement occurs mainly at areas with greater snow depth over the palsa. The result also reflects the influence of air temperature and wind on the distribution of snow over the palsa, where the northeastern parts of the ridge-shaped palsa have a greater snow depth and the top of the palsa completely lacks snow.

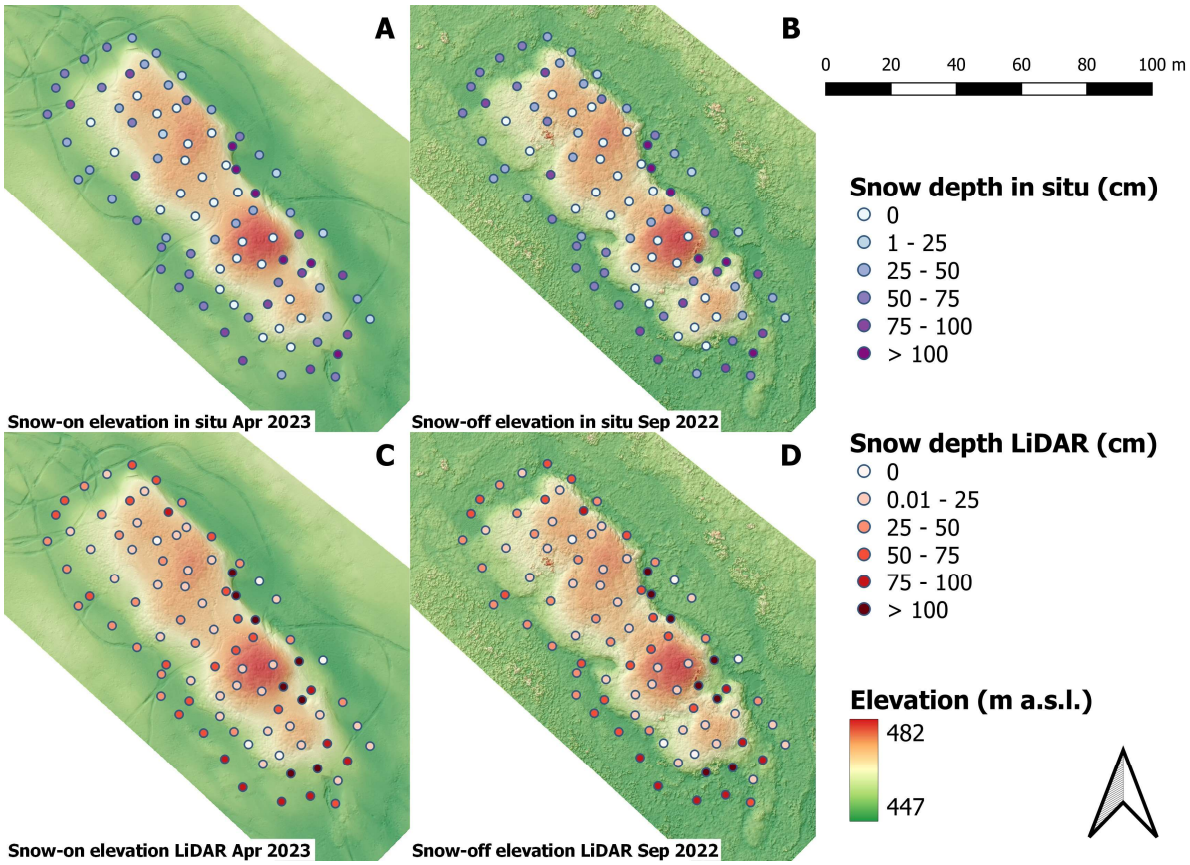

Figure 9. Snow depth measurements taken over the ridge-shaped palsa. A) in situ snow-on elevation model layer; B) In situ snow-off DTM layer; C) LiDAR snow-on elevation model layer; D) LiDAR snow-off DTM layer. The in situ measurements were taken on 19th April 2023.

Figure 10 shows snow depth measurements overlaid on the orthophotos taken over the ridge-shaped palsa. The snow-on orthophotos taken 18th April 2023 show the difficulties in measuring the snow depth over a palsa in situ, as it is difficult to know the palsa topography and where the height limits of the pals go. Compared with the snow-off orthophotos in Figure 10B & D, a lot of the topoghraphy of the ridge-shaped palsas edges is hidden under the snow, while the snow-on orthophotos in Figure 10A & C also have snow-free areas at the top of the palsa. By placing the snow depth points over the snow-off orthophoto, it can be more easily illustrated where over the ridge-shaped palsa topography each measurement has been carried out. This results in many answers to why the greater part of the ridge-shaped palsa has its deepest snow points in the northeastern area because there is a greater difference in elevation there.

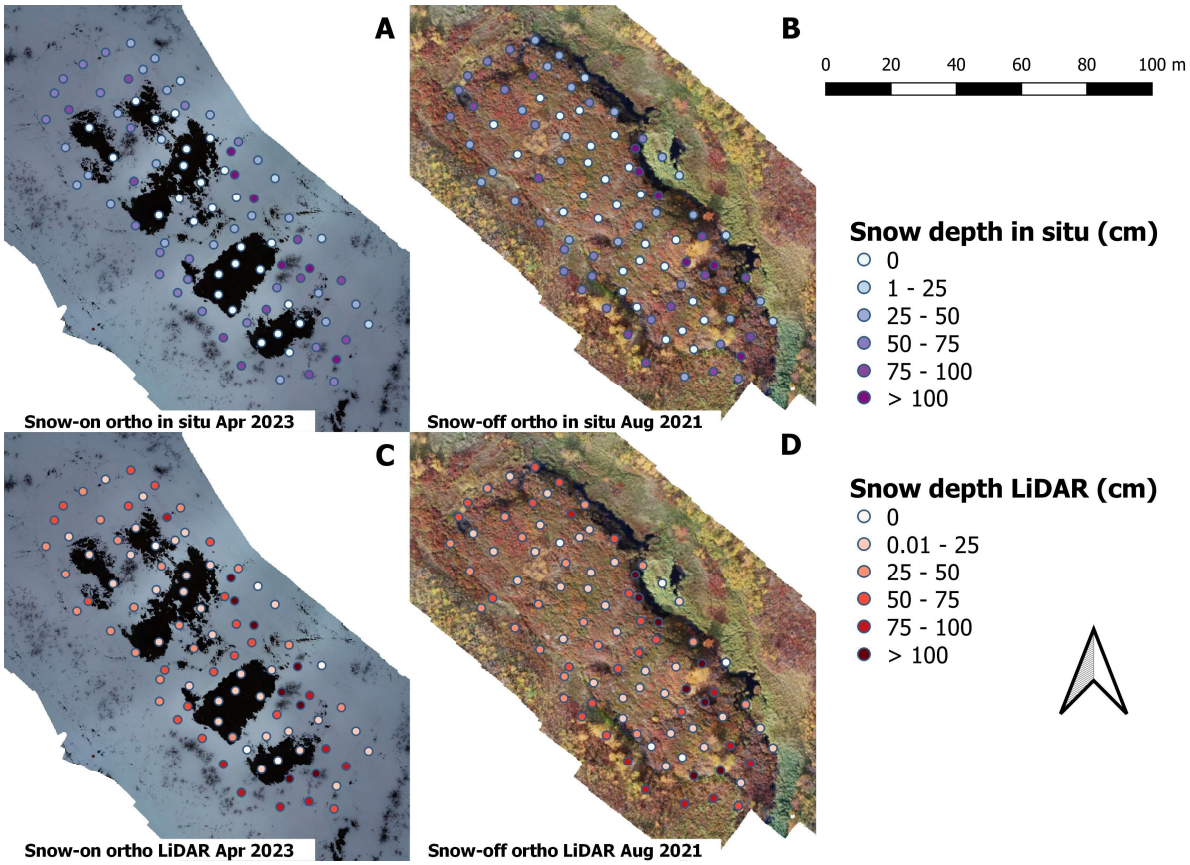

Figure 10. Orthophotos taken over the ridge-shaped palsa showing snow depth points. A) in situ points on snow-on ortho; B in situ points on snow-off ortho; C) LiDAR points on snow-on ortho; D) LiDAR points on snow-off ortho. The snow-on orthophoto was taken 18th April 2023.

Figure 11 shows the in situ snow depth and the LiDAR measured snow depth on the dome-shaped palsa. Most of the deeper measuring points can be found at the eastern edges of the dome-shaped palsa and a couple of deep holes at its northern edge. The dome-shaped palsa also has a smaller road that crosses over and cuts into the topography of the palsa. This can be discerned in Figure 11B & D. Here, greater snow depths can also be found from both snow depth measurement methods.

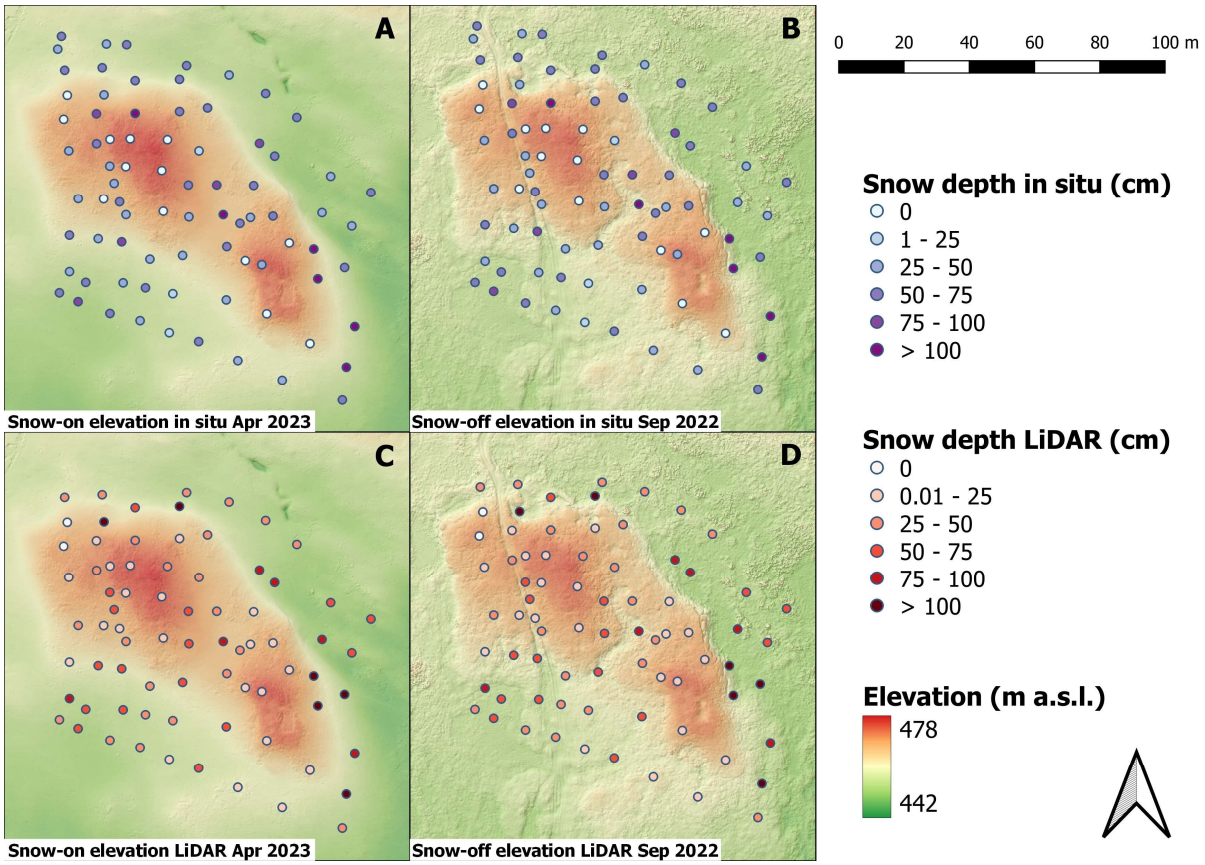

Figure 11. Snow depth measurements taken over the dome-shaped palsa. A) in situ snow-on elevation model layer; B) In situ snow-off DTM layer; C) LiDAR snow-on elevation model layer; D) LiDAR snow-off DTM layer. The in situ measurements were taken on 18th April 2023.

Figure 12 shows snow depth measurements for the dome-shaped palsa overlaid on orthophotos taken over the palsa. As with the ridge-shaped palsa, the snow-on orthophoto taken 20th April 2023 shows the difficulties in relating to the area and topography of the palsa when it is covered by snow on the edges of the dome-shaped palsa. The orthophotos illustrate a good overview of the topography as with the ridge-shaped palsa in Figure 10 and the east parts of the dome-shaped palsa have steeper topography. Since there is lack of stereo photo coverage in Figure 12A & C, some parts in the middle of the dome-shaped palsa is missing.

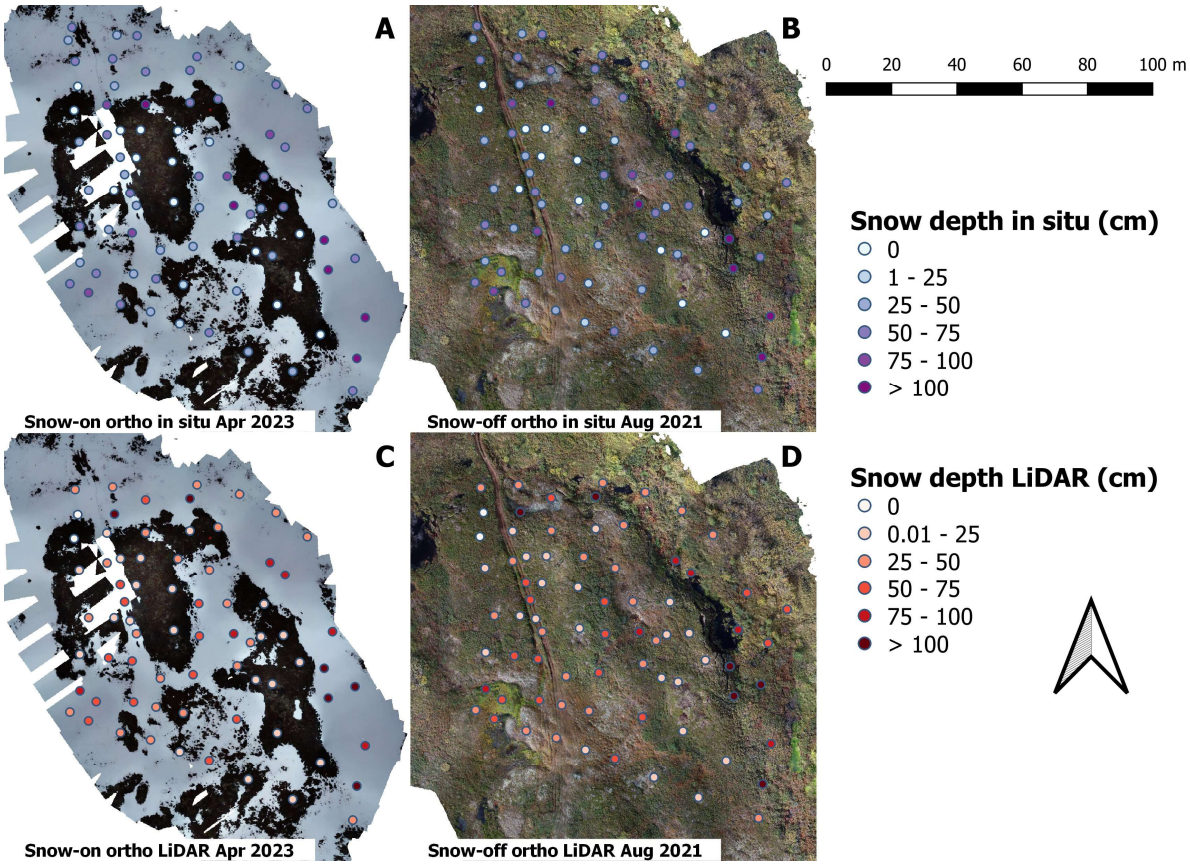

Figure 12. Orthophotos taken over the dome-shaped palsa showing snow depth points. A) in situ points on snow-on ortho; B in situ points on snow-off ortho; C) LiDAR points on snow-on ortho; D) LiDAR points on snow-off ortho. The snow-on orthophoto was taken 20th April 2023.

3.1.1 Snow depth data analysis

Figure 13 shows two scatter plots of the results from the regression analysis performed between snow depth values in situ and snow depth values calculated with LiDAR. The regression line is presented as a straight line with the function for each line. The function of the linear regression is shown for both the regression analysis over the ridge-shaped and dome-shaped palsas. A 1:1 line in black representing the $y = x$ is also presented.

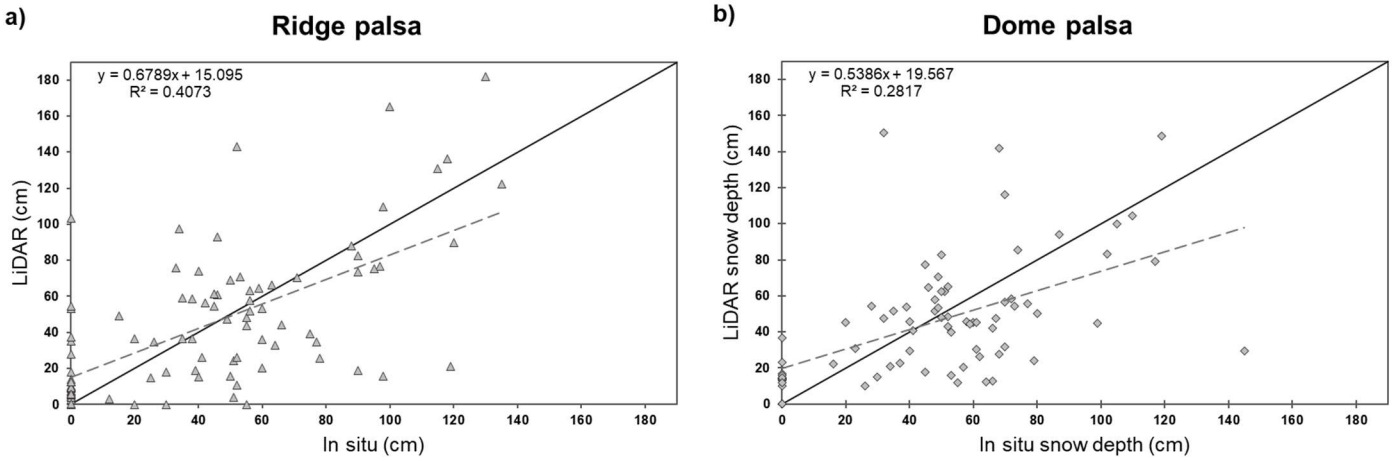

Figure 13. Linear regression and correlation analysis over the in situ and LiDAR snow depth measurements taken on a) the ridge-shaped palsa; b) the dome-shaped palsa.

In Table 1, the R^2 for the snow depth variables over the ridge-shaped palsa were calculated to 0.41 (0.4073) and for the dome-shaped palsa snow depth variables, the R^2 was calculated as 0.28 (0.2817). The p-value between the snow depth measurements for both the ridge-shaped and dome-shaped palsas was calculated to very low values, 1.0107E-11 for the ridge-shaped and 9.67341E-07 for the dome shaped palsa, indicating that the correlations is statistically significant. The observation number represents the same number of observations performed in situ with the same number of calculated LiDAR snow depth measurements at each measured point. The RMSE values for the ridge-shaped and dome-shaped palsas where both high and it was higher for the data over the ridge-shaped palsa (30.28) than over the dome-shaped palsa (27.64).

Table 1. The correlation coefficient (R), p-value, RMSE and number of observation points for snow depth over the ridge-shaped and dome-shaped palsas.

	Ridge-shaped palsa	***Dome-shaped palsa***
Multipel R	0.64	0.53
R^2	0.41	0.28
p-value	1.0107E-11	9.67341E-07
RMSE	30.28	27.64
Observations	91	75

Figure 14 shows a boxplot of all snow depth measurements over the ridge-shaped and dome-shaped palsas. The boxplot illustrates the mean, median, maximum and minimum value as well as the upper and lower quartile. The lower quartile (the lower edge of the boxes) marks 25% of all snow depth measurements, while the upper quartile (the upper edge of the boxes) represents 75% of the snow depth measurements. Each "box" contains 50% of all snow depth measurements. The values on the "whiskers" outside the box represent outlying values, and points at the far end are considered outliers, usually about min and max values.

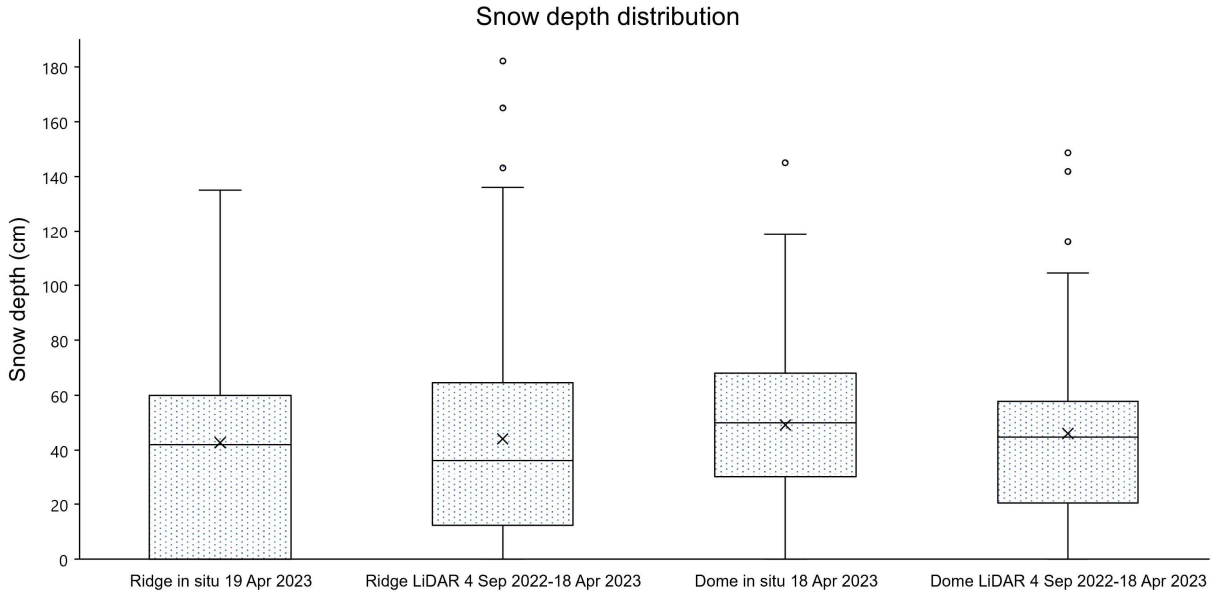

Figure 14. Boxplot showing the in situ and LiDAR snow depth measurements over the ridge-shaped and dome-shaped palsas. The box represents 50% of all measurements from each site and method. The

Black cross in the box represents the mean and the black line in the box the median value. The black circles show the outliers, the highest values in each set of measurements.

The results of the data analysis from all snow depth measurements over the ridge-shaped and dome-shaped palsas were compiled in Table 2. The data values shown in Table 3, such as the mean and median value as well as the maximum and minimum value for the snow depth, can be read in a slightly simplified manner in Figure 14.

Table 2. Summarized statistics for in situ and LiDAR snow depth between the ridge-shaped and dome-shaped palsas.

	In Situ Ridge SD (cm)	*LiDAR Ridge SD (cm)*	*In Situ Dome SD (cm)*	*LiDAR Dome SD (cm)*
Mean	42.68	44.07	49.16	46.04
Median	42.00	36.25	50.00	44.75
Standard Deviation	37.18	39.55	32.36	32.84
Minimum	0	0	0	0
Maximum	135.00	182.06	145.00	150.49
Observations	91	91	75	75

3.2 Weather data

Figure 15 shows the air temperature where a constant pattern for winter and summer time can be observed. The mean value calculated between Naimakka and Kilpisjärvi which was considered to represent air temperature at Saarikoski best, is presented between 2017-01-01 to 2022-09-05. After that, the air temperature from the Saarikoski weather station can be read out until 2023-04-22. The air temperature from GU's field station in Saarikoski follows approximately the same variation in air temperature as for previous yearly periods 2017-2022. The maximum and minimum temperature over the whole period were +21.9º C and -33.9º C respectivley.

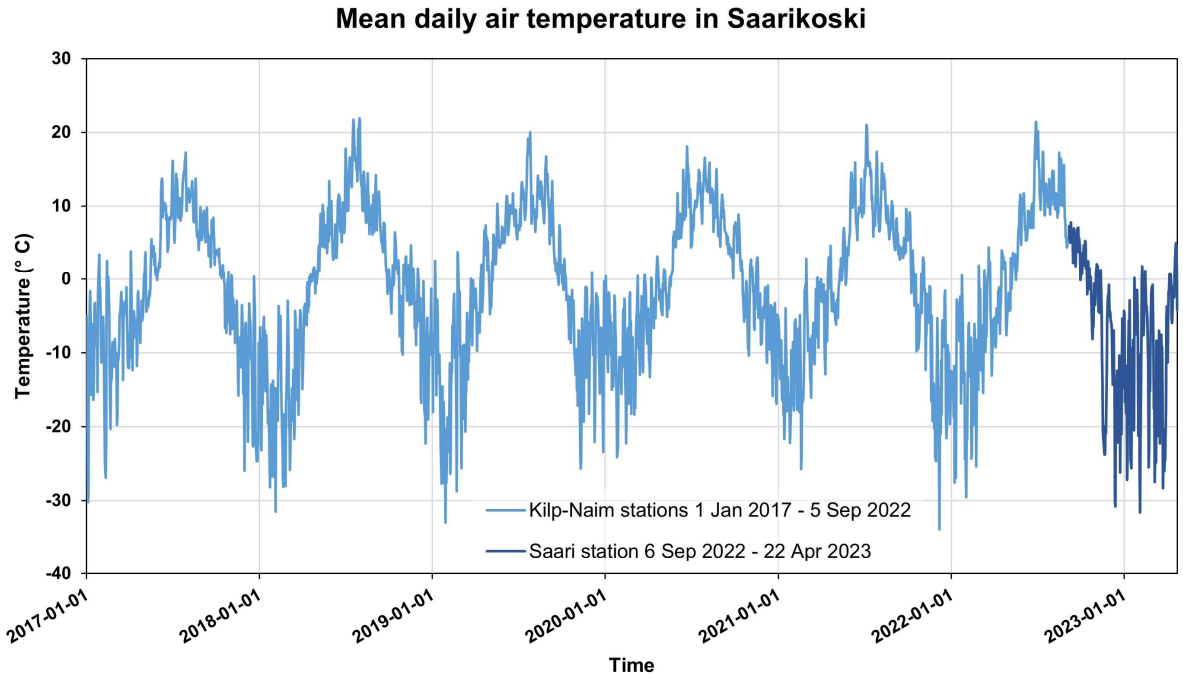

Figure 15. Mean daily air temperature in Saarikoski based on mean air temperature values from Kilpisjärvi and Naimakka connected to the Saarikoski weather station.

A data analysis between the air temperature at GU's field station in Saarikoski and between the calculated air temperature from Naimakka-Kilpisjärvi stations resulted in a scatter plot, to illustrate the relationships between variables (Figure 16). The scatter plot also shows a regression line through all point values, which represents the function according to Eq 1. The correlation was considering a positive correlation, due to its high value of 0.98. The P-value was calculated to be 5.3E-199, which shows that the correlation between Naimakka-Kilpisjärvi daily mean temperature and Saarikoski daily mean temperature is statistically significant. A 1:1 line in black was also made for better comparison.

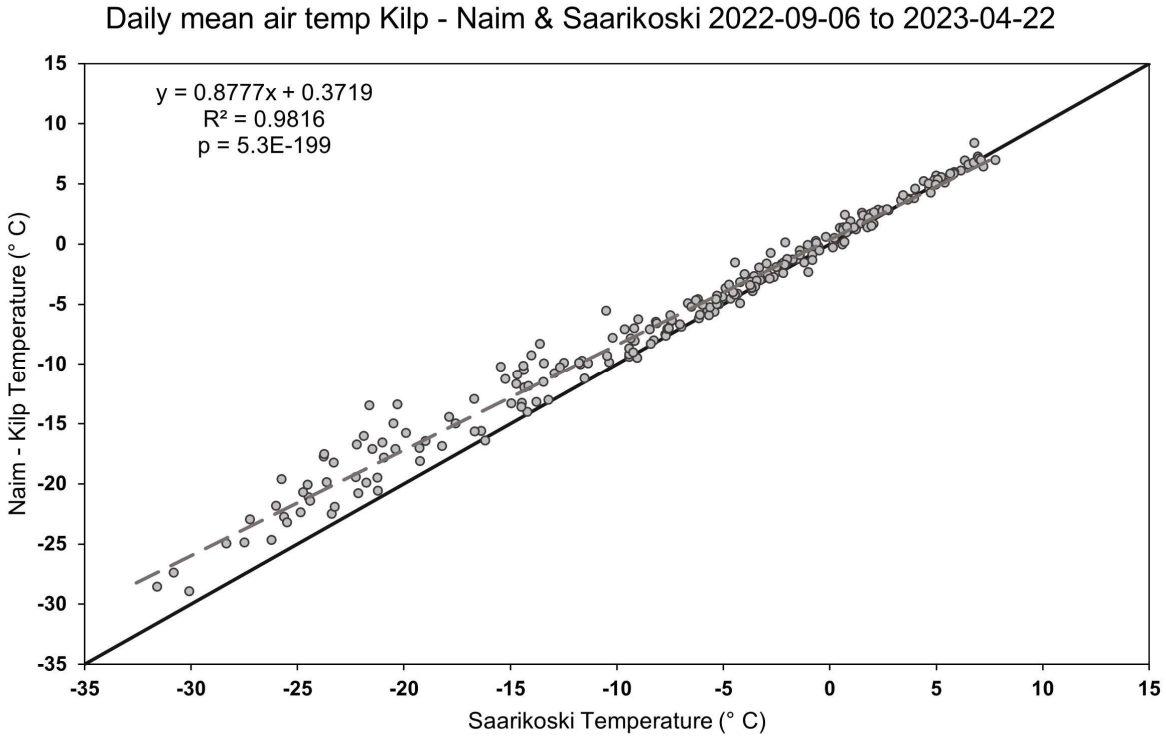

Figure 16. Scatter plot showing the linear regression between the Saarikoski field station daily mean air temperature and the Naimakka-Kilpisjärvi daily mean air temperature, as well as the correlation coefficient squared value (R^2).

All values from the data analysis of the air temperature in Figure 16 were summarized and entered in Table 3. The daily mean air temperature between Naimakka-Kilpisjärvi and Saarikoski does not show any major differences either in min-max values, median or average value.

Table 3. Statistical distribution over the daily mean air temperature in Naimmakka-Kilpisjärvi and Saarikoski stations.

	Temp mean Naim-Kilpis	***Temp Saarikoski***
Mean	-6.1	-7.4
Median	-4.7	-5.3
Standard Deviation	8.5	9.6
Minimum	-28.9	-31.6
Maximum	8.4	7.8

The monthly climatology for the years 2017-2022 is presented in Figure 17. The climatology shows an average temperature for every month that was calculated for each year of 2017-2022. The climatology presents which months had the lowest and highest air temperature during the studied years. For the months April-June, it is shown that the temperature reaches above 0º C which were the months used as the reference period when trying to find the first snowmelt dates in the optical satellite imagery. Temperatures are warming after February and cooling after August, which can be seen in Figure 17.

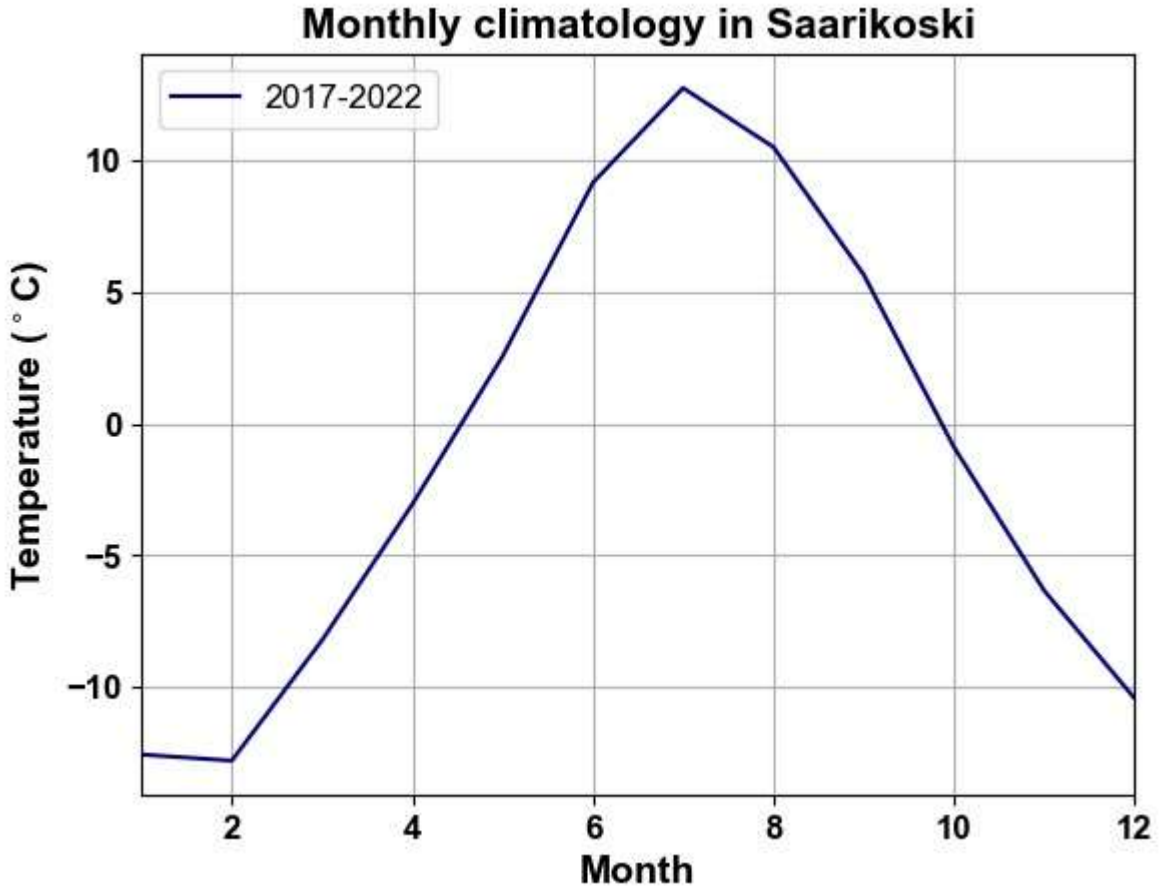

Figure 17. Monthly climatology in Saarikoski shows the mean air temperature for each month over the years 2017-2022. The temperature indicates that over the six observed years, the first snowmelt should begin around the 4th to 6th months (April-June).

Figure 18 shows the annual air temperature for the months of April, May and June for 2017-2022. The result is based on the monthly climatology for the assumed first snow melting period. The average temperature for April is below 0º C for all years, while May and June are above. For May and June, the temperature was almost the same in 2018. After that, the difference between the average temperature for the two months increased.

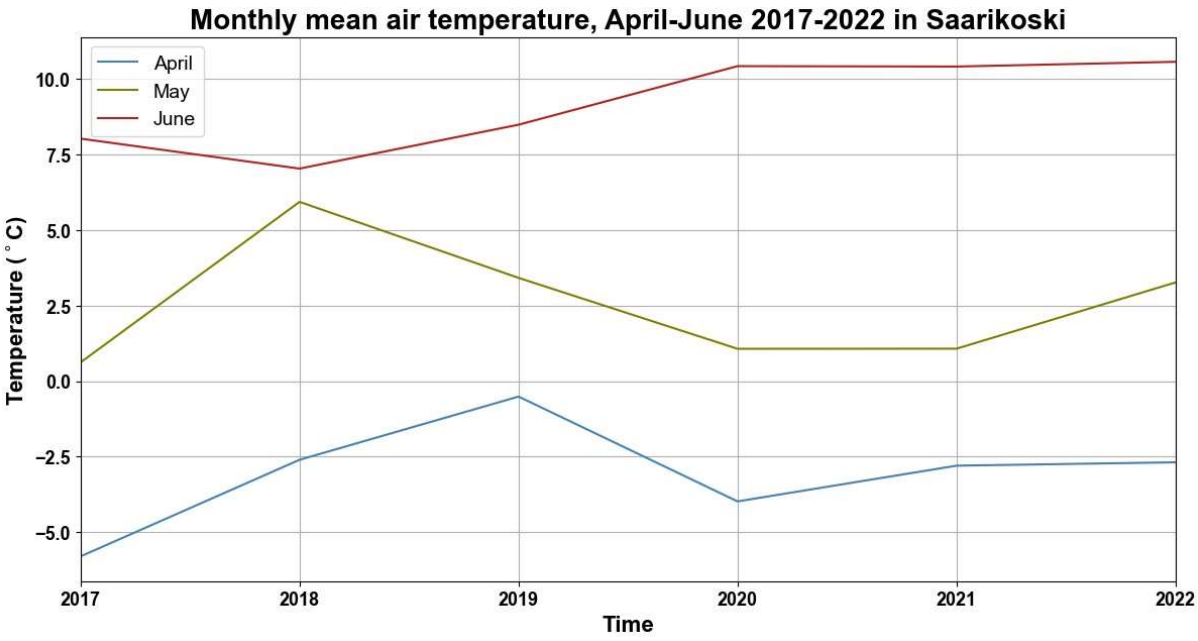

Figure 18. Monthly mean air temperature for April, May and June for the years 2017-2022 in Saarikoski.

Figure 19 shows a wind rose plot of wind direction and wind speed in Naimakka for the years 2017-2022. The wind rose is shown as a circle where different "spokes" show the frequency of wind directions over the 6-year period. The length of each staple shows how common the direction is per unit of time. It can be read that 17.5 % of the winds come mainly from west, and northwest (WNW) followed by east (E, 15 %) and north (N, ca 10 %). A minority of the winds come from the southwest (SW) and northeast (NE) while winds from the south are almost completely absent.

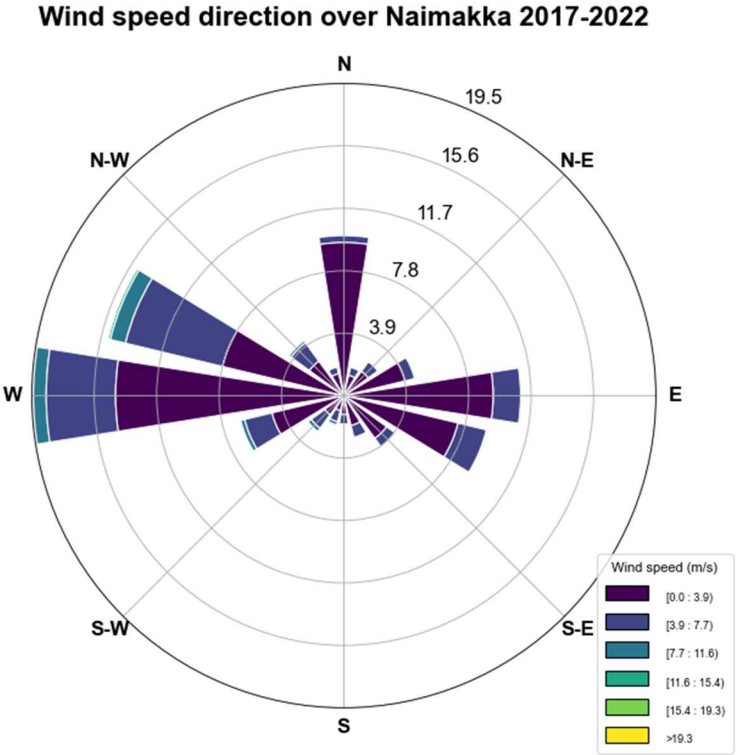

Figure 19. Wind direction and wind speed in Naimakka during the years 2017-2022.

3.3 Optical satellite data

Some of the 23 satellite images taken from Sentinel-2 are presented in Figure 20. Figure 20A shows a Sentinel-2 image taken during the first snowmelt over both the ridge-shaped and dome-shaped palsas on 2022-04-20. It is mostly the tip of the ridge-shaped and the dome-shaped palsas that can be visible. In Figure 20C, the ridge-shaped and dome-shaped palsas both have snow around its western sides, and on the dome-shaped palsa there is still snow around the southern area of the palsa. On top of both the ridge-shaped and the dome-shaped palsas, it can be seen as completely snow-free. The snow-free date for both palsas in Figure 20C was from the year 2017-06-1-09. The satellite image in Figure 20B taken nine days after the first snowmelt date in Figure 20A, is not a first snowmelt or snow-free date, but only shows how the snow slowly melts over the ridge-shaped and dome-shaped palsas between the first snowmelt and snow-free dates.

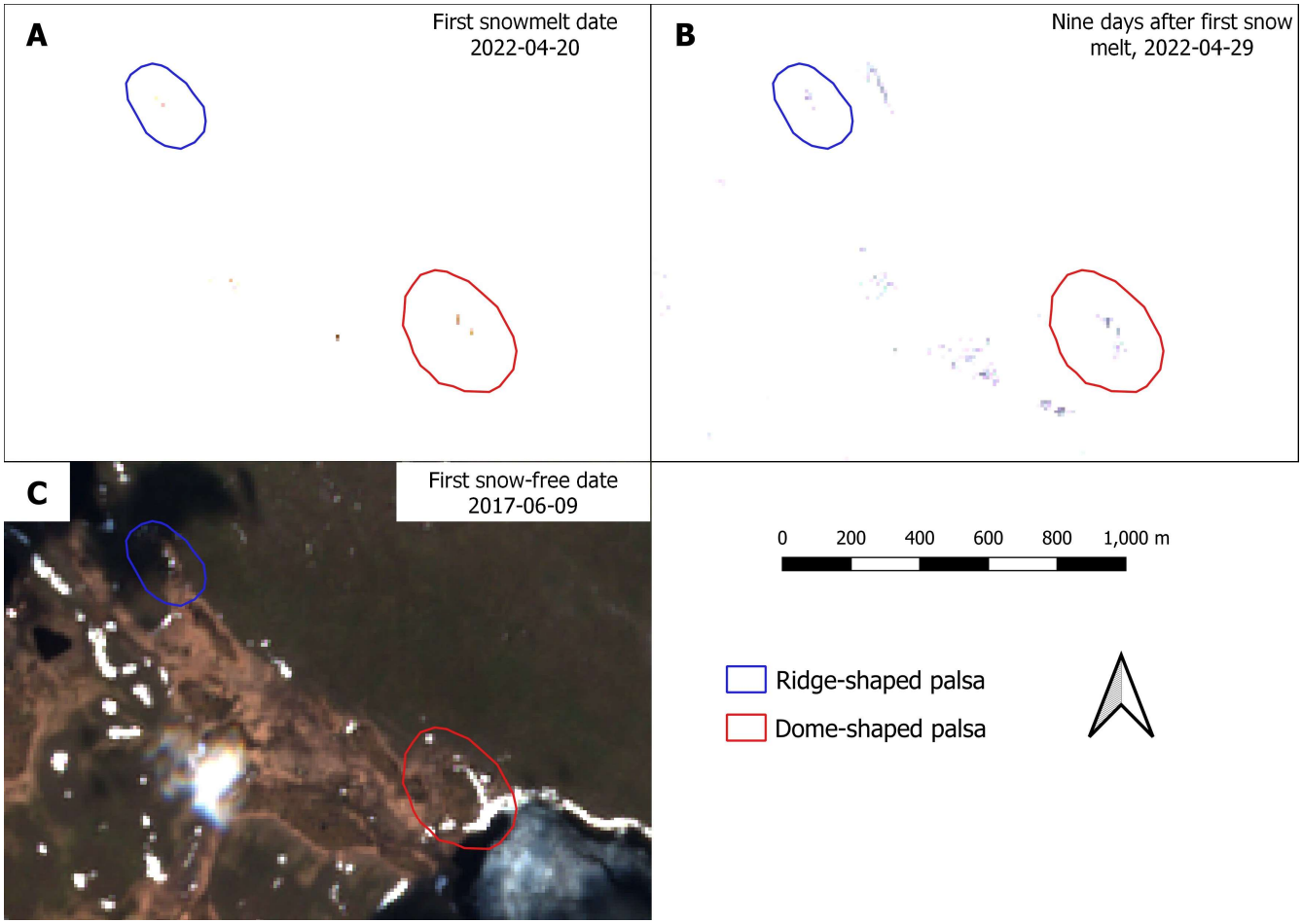

Figure 20. Sentinel-2 images taken over Vissátvuopmi showing how the first snowmelt and snow-free date over the ridge-shaped and dome-shaped palsas look for different years. A) the first snowmelt date for both the ridge-shaped and the dome-shaped palsas 2022-04-20; B) nine days after first snowmelt date, 2022-04-29; C) first snow-free date of the year 2017-06-09. Source: Copernicus Open Access Hub, 2023.

For each year between 2017-2022, a first melt date was extracted for the ridge and dome palsas and a first snow-free date for the ridge and dome palsas was taken which was put into Table 4. In some cases, the given dates are only an estimate as clouds covered most of the palsas during the first melted and free snow period.

Table 4. First snowmelt date for each palsa as well as first snow-free date based on Sentinel-2 satellite images.

Year	Ridge palsa first snowmelt	Ridge palsa snow-free	Dome palsa first snowmelt	Dome palsa snow-free
2017	3 May	9 June	16 May	2 June
2018	26 April	21 May	25 April	16 May
2019	15 April	10 May	18 April	10 May
2020	21 April	8 June	22 April	30 May
2021	17 April	4 June	19 April	1 June
2022	20 April	30 May	20 April	26 May

Figure 21 shows a plot of the first snowmelt and first snow-free dates for the satellite analysis from Table 4. The days of the year (DOY) is represeting the exact day number of each year from 2017-2022. The period between the first snowmelt and the snow-free dates can be illustrades as the snow melting time, and had it lowest time period of 2019, where the snow melting time for the ridge-shaped palsa was approximately 25 days and for the dome-shaped palsa around 22 days. After 2019, the snow melting period for both the ridge-shaped and dome-shaped palsa is shown to have increased, being at its highest in 2021. The first snowmelt date over both palsas has also started to occur earlier in the spring since 2017.

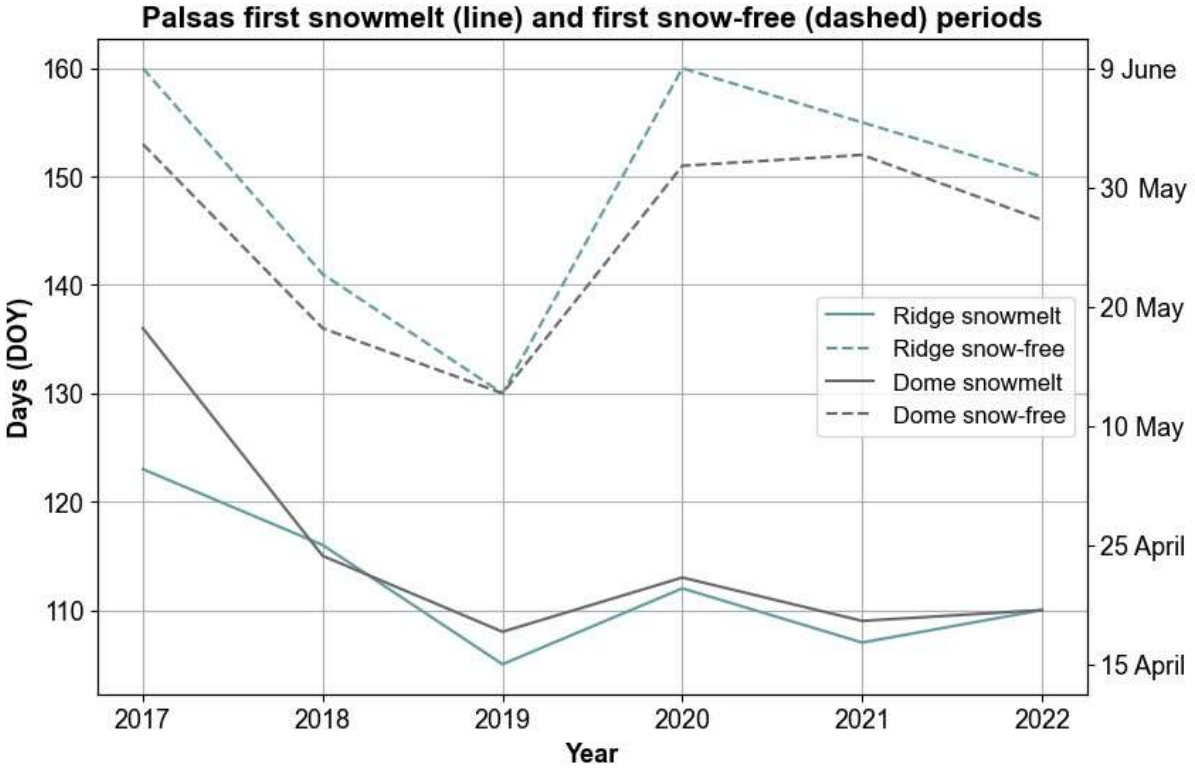

Figure 21. Days of the year (DOY) when the first snowmelt and the first snow-free dates occur over the ridge palsa and dome palsa with the help of optical satellite images from Sentinel-2.

4. Discussion

This section discusses the results and the methods performed and presented for the study, as well as comparing with previous examinations and described literature of similar studies.

4.1 Discussion of the results

4.1.1 UAV LiDAR and in situ snow depth

The comparison of how well the UAV LiDAR snow depth agrees with the in situ snow depth layer between 4th Sep 2022 – 18th Apr 2023 (Figure 8) looked good at first, and the in situ snow depth values seemed at the moment to be in relatively good agreement with the LiDAR snow depth measurements, even though it was known that the point location of the LiDAR was much more accurate (2cm) as compared to the location of the in situ data that was taken using the smartphone GPS (4-9m). When the in situ and LiDAR values were placed in a scatterplot (Figure 13a-b) to find a relationship, the correlation for the ridge-shaped palsa snow depth values were shown to be intermediate (0.41), where in the dome-shaped palsa values, it was shown to be below intermediate (0.28). In contrast, a relatively large spread of points in the snow depth variables was demonstrated in Figure 13a-b. This indicates that even when the snow depth variables were plotted, an overestimation of the expected correlation value was shown.

A likely reason why the correlation turned out to be lower than expected when the measurements over the ridge-shaped and dome-shaped palsas were compared would be the precision difference between the smartphone GPS and the UAV LiDAR RTK. Since smartphone GPS has a precision of between 4-9 m and RTK a precision of 2 cm, the differences in precision level between them are very high. If Emlid Reach RS2 GPS had been used instead of smartphone GPS, it is likely that the correlation between UAV LiDAR and in situ measurements would have been more positive. The results of the snow depth measurements showed that there were generally quite similar intervals of measurements between in situ and LiDAR and, moreover, they were statistically significant.

When looking and comparing the RMSE values for the ridge-shaped and dome-shaped palsas in Table 1, it is shown that the RMSE values for both palsas are high, indicating that the model has more errors and less precise accuracy than it looks when comparing in situ and LiDAR snow depths in Figure 8. It might also indicate that the models are biased. In contrast to the correlation, the RMSE for the ridge-shaped palsa (30.28) was higher than for the dome-shaped palsa (27.64), indicating that the model for the ridge-shaped palsa is less accurate and has higher errors compared to its correlation which is higher than the dome-shaped palsa. Since the correlation was higher for the ridge-shaped palsa, the RMSE should be lower than the RMSE for the dome-shaped palsa. One reason why the RMSE is slightly higher for the ridge-shaped palsa could be that the distribution of data values may be slightly more spread out than for the dome-shaped palsa (Figure 13a-b), which may have contributed to higher error values. Some of the outlier data points observed in Figure 13a-b does not really hang with the rest of the more scattered data points and is most likely the reason to the high RMSE value for both the ridge-shaped and the dome-shaped palsas.

The snow depth statistics analysis result of the Figure 13a-b and Table 1 showing the linear regression and correlation analysis as well as the correlation coefficient of the snow depth over the two palsas was based on the same method as described in two other papers (Feng et al., 2023; Proulx et al., 2022). According to the results in the study from Proulx et al. (2022) the authors was using a magnaprobe with a precision of less than 0.1 mm when they performed the in situ snow depth measurements for comparing with UAV LiDAR snow depth

measurements in a snow covered farmland/forestry area. Their result was a bit difficult to compare with this study due to the high precision of the magnaprobe. The authors do describe an overall correlation between the magnaprobe and UAV LIDAR measurements with an R^2 = 0.76 but in combination with a snow tube, which was a cylindric tube made of aluminum, which makes it difficult to compare with the correlations made in this study. For statistical analysis between snow depth measurements in situ and snow depth measured with UAV LiDAR, Proulx et al. (2022) presented a boxplot with statistical variables, something like the same boxplot in Figure 14. When the boxplot in Figure 14 is compared with the data in Table 2, it is observed that the snow depth measurements for LiDAR are within the same range over the ridge-shaped and dome-shaped palsas. Interestingly enough, the in situ measurements over the ridge-shaped palsa have the measurements that lie within the range of the boxplot. The many zero values in the in situ measurements taken over the ridge-shaped palsa can be explained by the fact that the measurements over the ridge-shaped palsa were taken one day after the other measurements, which contributed to lower readings as mild weather contributed to thawing of the snow for a short time.

In Feng et al. (2023) the authors describe a method that was more comparable with the methods used for snow depth comparison over the ridge-shaped and dome-shaped palsas, since they were using a stainless-steel ruler for in situ measurements snow depth distribution over periglacial landforms in the region of High Mountain Asia. For positioning point location, the authors used a CHCNAV RTK GPS with an accuracy of ± 2 cm and vertical range of ± 4 cm. Since system with very accurate precision was used, the results presented in Feng et al. (2023) shows a correlation with R^2-value of 0.90 and 0.85 between UAV LiDAR snow depth (cm) and in situ snow depth (cm), making up a very strong correlation. This might indicate that it could have been a similar correlation between the snow depth measurements over the ridge-shaped and dome-shaped palsas if the Emlid Reach RS2 GPS could have been used.

Based on analysis of data and mapping of snow depth over the ridge-shaped and dome-shaped palsas, correlation and linear regression analysis suggest that the lack of punctuality lies in the lack of precision of measurements performed in situ. The UAV LiDAR measurements must therefore be assessed as the most reliable method for performing snow depth measurements over the ridge-shaped and dome-shaped palsas. In Proulx et al. (2022), the authors also draw a similar conclusion when comparing and analyzing snow depth in situ with UAV LiDAR. For future studies of snow depth measurements in situ and with UAV LiDAR, it should be taken into account that high GPS precision is essential to achieve a good correlation between in situ and LiDAR measurements. The snow depth models might have had a lower RMSE if a bias correction was performed, which should be considered for future studies of the data. The result of this study also shows the necessity to be able to use LiDAR data in the future to investigate how well in situ measurements of snow depth agree with LiDAR, as LiDAR is a much more precise tool for measuring and calculating snow depth. Hopefully, future studies can be improved by how this study shows how big a difference different types of GPS precision can affect the results of snow depth between in situ and LiDAR measurements. It is also important that for similar studies in the future, more in situ measurements should be taken to better compare manual measurements with UAV LiDAR measurements, as more data can contribute to more concrete results.

4.1.2 Weather data and topography

For the air temperature analysis, both the monthly climatology (Figure 17) and the mean annual air temperature for Apr-Jun (Figure 18) was based on the daily mean air temperature

data in Saarikoski, (Figure 15). When comparing the air temperature from the Saarikoski station start from 2023-09-06, all daily averages were shown to follow roughly the same annual range as for the 2017 to 2021-2022 winter periods. To estimate how well the air temperature data from Saarikoski station relate to the calculated daily mean air temperature between Naimakka and Kilpisjärvi station, all daily mean values were plotted in a scatter plot (Figure 16) for the period 2022-09-06 to 2023-04-22. A correlation analysis from the scatterplot showed a very strong positive correlation, where R2 = 0.98. A very low p-value of $5.3E^{-199}$ indicates that the correlation is statistically significant. Statistical data from Table 3 also show small differences in mean, min and max temperature between both parameters. The correlation and p-value indicates that the calculated mean agrees relatively well with the calculated Naimakka-Kilpisjärvi mean.

One reason why the largest accumulations of snow on the ridge-shaped and dome-shaped palsas are just relative to the eastern parts of the two palsas is that the wind has helped to distribute the amount of snow. If the snow depth measurements are compared with the wind data from Naimakka (Figure 19) where most of the wind is blowing from a west southwest (WSW) to an east northeast (ENE) direction, there appears to be a similar relationship with the wind over the ridge-shaped and dome-shaped palsas. That the wind has affected the snow distribution and snow depth over the two palsas is supported by observations made in the field. At the ridge-shaped palsa, it could be demonstrated that snow has blown over the palsa in a west-east direction, which resulted in larger amounts of snow that have fallen down the steepest edge right in the middle of the eastern border of the ridge-shaped palsa (Figure 22).

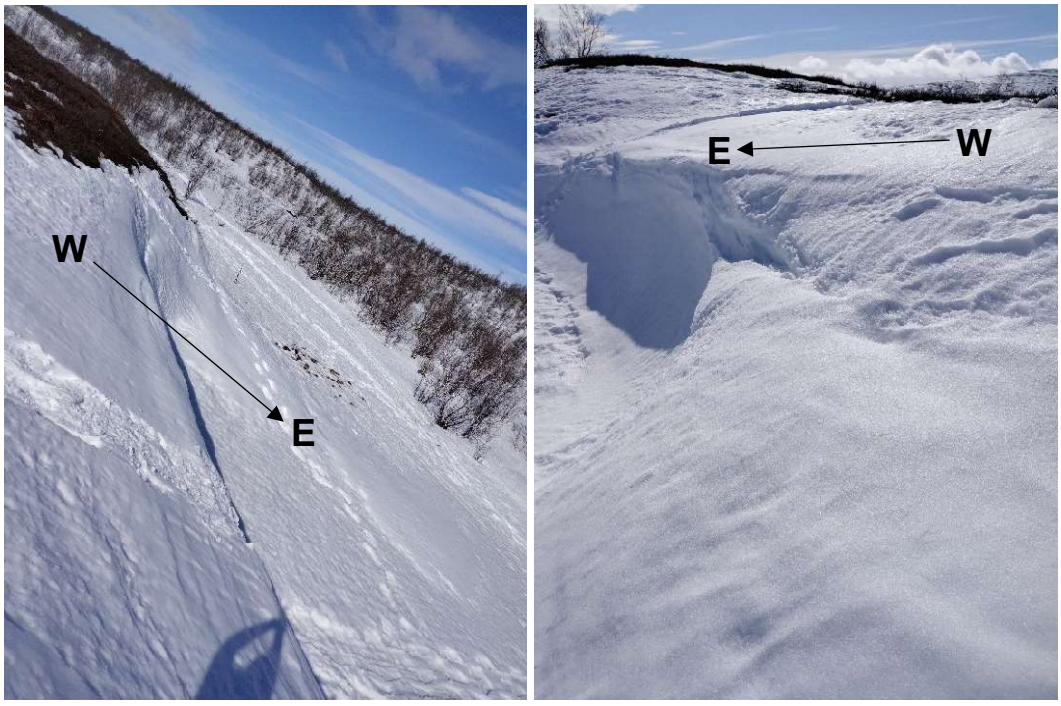

Figure 22. The steep east middle of the ridge-shaped palsa showing the snow being pushed over by the wind. The wind is shown from west (W) to east (E) direction.

At the dome-shaped palsa, a similar snow distribution could also be seen, but as the dome-shaped palsa is more hemispherical and not as steep around the edges as on the ridge-shaped palsa, it was not as easy to see the influence of the wind in the snow. Some parts of the

northeast side of the dome-shaped palsa does however show some track of wind impact (Figure 23).

Figure 23. Picture taken at the northeast border of the dome-shaped palsa, April 2023. Photo: Cas Renette.

The influence of the wind on the snow distribution over a palsa is described by Kujala et al. (2008) as "the wind carries snow and deposits it on the slope and elsewhere on the flat mire surface" which describes the results observed and measured on the ridge-shaped and dome-shaped palsas quite well. Sannel (2020) also described the results of their study as the wind being a major factor in snow distribution across the permafrost landscape since the wind redistribut snow across the permafrost mires.

Comparison of the snow depth measurements over the ridge-shaped and dome-shaped palsas shows that topography together with wind plays a significant role in how the snow depth is distributed over the two palsas. Since both the ridge-shaped and dome-shaped palsas had relatively flat slopes over its southwestern sides and steeper slopes on the eastern sides, it was with some expectation that the largest snow depths turned out to be around this side of the two palsas. Kujala et al. (2008) describes that this is what characterizes snow accumulation over a palsa and that snow-free peaks are present on top of the palsas and thicker snow collections lower down, usually surrounding the palsas. The elevation differences illustrated in Figure 9 and Figure 11 over the ridge-shaped and dome-shaped palsas show how the relationship between the topography of the height and the snow depth is. The highest areas on the top of the ridge-shaped and dome-shaped palsas were essentially completely snow-free, while the largest part of the snow accumulated down to the lower elevations and around the sides of the ridge-shaped and dome-shaped palsas.

At some places on the top of the ridge-shaped and dome-shaped palsas, there could be snow depths of between 75 up to over 100 cm, where it is assumed to be much less. Both in situ measurements and the LiDAR measurements demonstrated that on top of the palsa there were topographic elevation differences that contributed to the large snow depth values. For the ridge-shaped palsa, the same large snow depth measurements could also be measured on the

palsa's higher elevation, when there should be very low snow depths on the top of the palsa. Both the in situ measurements and the LiDAR measurements demonstrated that on the southern elevation of the ridge-shaped palsa there were topographic elevation differences that contributed to the large snow depth values.

The reason why these topographical differences can occur over the palsas according to Sannel et al. (2016) is that thick snow cover over the palsa produces more meltwater in the spring, which increases soil moisture and thus affects the thermal conductivity of the soil, which can result in warmer ground under the palsa's snow cover. On top of the ridge-shaped and the dome-shaped palsas, rough terrain was detected, which contributed to the uneven distribution of snow, where thick layers of snow contributed to creating depressions in surface (Sannel et al., 2016). In a previous study, Seppälä (2003) has shown that due to snow's low thermal conductivity, increased snow depths over peat and palsa ground resulted in higher ground temperature since a thick snow cover contributes to reduced heat flux from the soil. This may indicate that areas of deeper snow may cause an increase in soil moisture over the ridge-shaped and dome-shaped palsas. This was already shown in a study by Verdonen et al. (2023) in the palsa mire complex of Laassaniemi, Kilpisjärvi, 33 km from Vissátvuopmi. Verdonen concluded that the Laassaniemi palsa mire areal had its greatest loss during the years 1985-2000, where the snow depth was thickest and snow cover duration as longest over the Laassaniemi. Even if this study uses a much more present year, a recurring deep snow depth over the ridge-shaped and dome-shaped palsas in Vissátvuopmi can also contribute to reduced area over the two palsas. More snow depth studies over the Vissátvuopmi palsa mires need to be carried out for drawing further conclusion.
The snow-off elevation gives a good overview of the topography without snow and when the snow depth points are superimposed, it becomes easier to understand why the snow was so deep in certain places, and why it was thinner on top of the palsas. For example, the dome-shaped palsa in Figure 11 was assumed to be relatively snow-free at the top, but snow depth measurements in the field showed that some areas up on the top had quite large snow depths. One place on the dome-shaped palsa, that had a greater snow depth was on the ATV track that "cuts" through the middle of the dome-shaped palsa from north to south, forming a long narrow depression through the entire dome-shaped palsa (Figure 12B & 12C) By comparing the snow-on and snow off elevation, it was seen that under the snow layer on the dome-shaped palsa there were topographic elevation differences and depressions, where there could be snow depths of 75 to over 100 cm, where it is assumed to be much less.

4.1.3 Optical satellite data

Based on the weather data and optical satellite data it could be seen that for each year since 2017, the first snowmelt over the ridge-shaped and dome-shaped palsas started earlier in the spring (Table 4). It could be seen that since 2019, the first snow-free day has occurred later in the season, which has contributed to a very long snowmelt period over the two palsas. Even though it was often difficult to obtain cloud-free satellite data, the days where the first snowmelt and snow-free days could be clearly seen since snow has a clear spectral signal in the optical domain (Winsvold et al., 2016). Except for 2018 and 2022, the first snowmelt occurred on the ridge-shaped palsa first. The first snowmelt date for the dome-shaped palsa occurred not so long after. This might have to do with the fact that the ridge-shaped palsa is much steeper around its edges, which can contribute to the snow accumulating there a little earlier. It might also be that the ridge-shaped palsa is more exposed to wind. This may have something to do with the fact that the ridge-shaped palsa has decayed much more area-wise (over 50%) than the dome-shaped palsa, which has decayed by about a third in the last 63-64 years (Olvmo et al., 2020). Since the ridge-shaped palsa is narrower on the leeward side

compared to the dome-shaped palsa, it might be assumed that the height differences play a role in how the snow melts on top of the ridge-shaped palsa and the dome-shaped palsa accumulates (Olvmo et al., 2020).

It could be seen from the optical satellite images like in Figure 20 how the snow cover on and around the ridge-shaped and dome- shaped palsas usually melts down to only having an accumulation of snow around its lowest elevation, which was also described by Kujala et al. (2008) as characteristic of a palsa hill. In the ridge-shaped palsa, a smaller accumulation of snow can be found behind its steep, eastern edge, which is probably since the steep palsa ridge gives the snow shade and therefore it melts more slowly on that side. Around the dome-shaped palsa, the snow depth points in Figure 9-12 show that the snow depth is greatest at the eastern, north-eastern and southeast part of the palsa, which can also be observed on satellite images (Figure 20).

A study by Dietz et al. (2011) using remote sensing was made over snow cover variability in Torneälven area, located around the Swedish-Finnish border and close to Vissátvuopmi palsa mire complex, showing an interesting relationship with the analysis in Figure 21. According to the study, the authors predicted how the snowmelt runoff in Torneälven could drastically increase from 400 discharge (Q1[m^3/s]) in 2001 to over 1000 in 2018 (Q1[m^3/s]). The period for the discharge has also increased, starting in the beginning of May and end first in September. The result from the satellite data analysis may indicate that the connection for the discharge period in 2018 and the period when the snowmelt on the ridge-shaped and dome-shaped palsas also increases. However, the results should be taken with some caution, as the article was published in 2011 and calculated future scenarios, while the results of the satellite data analysis are contemporary observations. However, more comparisons between the snowmelt period of Vissátvuopmi and snowmelt causing the higher discharge could be performed for further analysis.

4.2 Discussion of the methods

During the execution of the project, certain parameters have been considered, that might have changed the outcome of the project. These should be taken into account for future use of this project. The parameters that could change the outcome of the result and the execution are:

A. *Air temperature change for days between the measurements* - Since the snow depth measurements are carried out on different dates, where the snow depth on the dome-shaped palsa was measured one day before (18 Apr) the ridge-shaped palsa (19 Apr). The period when the study in Vissátvuopmi was carried out was unusually warm, and according to SMHI ("n.d."), air temperatures were several degrees above the normal mean temperature for April. This has most likely contributed to the fact that the snow depth measurements over the ridge-shaped palsa decreased by a few centimeters, as it could already be estimated that the air temperature was warmer on 19 April.

B. *Errors with the Emlid Reach RS2 GPS battery and GPS precision* - The aim was to initially use an RTK-GPS for precision measurements for each location of each snow depth measurement in situ, but when the battery life proved to be insufficient when mapping the dome-shaped palsa, it was decided to use the Qfield in the smartphone instead. The precision of a modern smartphone is 4-9 m and an Emlid Reach RS2 GPS has a precision of 2 cm in good conditions, making it most likely that the correlation

and precision between the in situ and LIDAR snow depth would have been higher if the Emlid Reach RS2 GPS would have been in use instead.

C. *Data errors for climate data (missing months etc.)* – In some cases, the weather data was missing some values over its original dataset. This was mainly found in the Naimakka dataset air temperature and wind data. Since these values where only missing one month of data over 6 years and it was easy to calculate new mean values from earlier and later periods in the dataset, it was considered a minimal error that probably not would have make a big difference in the outcome.

D. *Cloud coverage when observing Sentinel-2 data* – A common problem when observing the dates in Sentinel Hub EO Browser is the cloud coverage and in some cases, this was a real obstacle when trying to find the first snowmelt and snow-free dates over the ridge-shaped and dome-shaped palsas. Because of this, some dates for the first snowmelt and snow-free periods had to be estimated, since cloud coverage before might have hidden the first snowmelt or snow-free image. Luckily, it was only a few times that the cloud cover was so extensive it resulted in having to make an estimation of the first snowmelt and snow-free date.

E. *Calculating LiDAR-diff* – Because the LiDAR snow depth layer is based on a calculated difference between two elevation layers, then difference assumption is made that the terrain elevation in September (snow-free) is the same as the terrain elevation in April (when covered with snow). With LiDAR, parameters such as vegetation, terrain and water accumulations can play a major role when an elevation model is created, something that can be avoided and mapped in situ. There are also parts where the LiDAR proves to be more precise, among other things because the precision is more accurate.

5. Conclusion

Remote sensing was used to study snow dynamics over a ridge-shaped and dome-shaped palsa, showing that it can provide different approaches to measure snow dynamics over a palsa. Although manual in situ measurements is relatively easy and quick to carry out, the use of UAV LiDAR has proven to be easier, faster and more efficient to measure snow dynamics palsa mires. Some of the conclusions of this study are:

- UAV LiDAR measurements of snow depth have very high precision and accuracy, which cannot be achieved by manual in situ measurements of snow depth over the ridge-shaped and dome-shaped palsas. Low intermediate correlation between the two measurements was shown, with an R^2-value of 0.41 for the ridge-shaped and 0.28 for the dome-shaped palsa. This was likely due to lower precision of the in situ measurements.

- The topography of the palsa in combination with air temperature and wind is some of the main factors controlling the distribution of snow dynamics on and around the ridge-shaped and dome-shaped palsas.

- Sentinel-2 data were useful in identifying the first snowmelt date and snow-free date but were sometimes not available due to cloud coverage. The first snowmelt date over the ridge-shaped and dome-shaped palsas has occurred earlier since the year 2017, while the first snow-free dates have started to occur later since 2019, resulting in a longer snowmelt period, for the ridge-shaped palsa about 15 days longer and dome-shaped palsa about 14 days longer in 2022 than in 2019.

Continued studies and mapping of Sweden's palsa mires are needed to increase the understanding about how ongoing climate change affects these sensitive landforms. Measurements of snow dynamics with remote sensing methods such as LiDAR and optical satellite images, are some of the most comprehensive methods to increase further knowledge of palsa mires in the future.

References

Aalstad, K. (2019). *Ensemble-based retrospective analysis of the seasonal snowpack* https://www.researchgate.net/publication/338423002_Ensemble-based_retrospective_analysis_of_the_seasonal_snowpack

Asuero, A. G., Sayago, A., & González, A. G. (2007). The Correlation Coefficient: An Overview. *Critical Reviews in Analytical Chemistry*, *36*(1), 41-59. https://doi.org/10.1080/10408340500526766

Borge, A. F., Westermann, S., Solheim, I., & Etzelmüller, B. (2017). Strong degradation of palsas and peat plateaus in northern Norway during the last 60 years. *The Cryosphere*, *11*(1), 1-16. https://doi.org/10.5194/tc-11-1-2017

Browser, S. H. E. ("n.d."). *EO Browser*. Retrieved April 25 from https://apps.sentinel-hub.com/eo-browser/?zoom=10&lat=41.91262&lng=12.50896&themeId=DEFAULT-THEME&toTime=2023-04-04T15%3A52%3A22.426Z

Copernicus. (2020). *Climate Change Service*. Retrieved 27 April from https://cds.climate.copernicus.eu/toolbox/doc/how-to/13_how_to_calculate_climatologies_and_anomalies/13_how_to_calculate_climatologies_and_anomalies.html

de la Barreda-Bautista, B., Boyd, D. S., Ledger, M., Siewert, M. B., Chandler, C., Bradley, A. V., Gee, D., Large, D. J., Olofsson, J., Sowter, A., & Sjögersten, S. (2022). Towards a Monitoring Approach for Understanding Permafrost Degradation and Linked Subsidence in Arctic Peatlands. *Remote Sensing*, *14*(3). https://doi.org/10.3390/rs14030444

Dietz, A. J., Kuenzer, C., Gessner, U., & Dech, S. (2011). Remote sensing of snow – a review of available methods. *International Journal of Remote Sensing*, *33*(13), 4094-4134. https://doi.org/10.1080/01431161.2011.640964

Dumont, M., & Gascoin, S. (2016). 4 - Optical Remote Sensing of Snow Cover. In N. Baghdadi & M. Zribi (Eds.), *Land Surface Remote Sensing in Continental Hydrology* (pp. 115-137). Elsevier. https://doi.org/https://doi.org/10.1016/B978-1-78548-104-8.50004-8

Feng, T., Hao, X., Wang, J., Luo, S., Huang, G., Li, H., & Zhao, Q. (2023). Applicability of alpine snow depth estimation based on multitemporal UAV-LiDAR data: A case study in the Maxian Mountains, Northwest China. *Journal of Hydrology*, *617*. https://doi.org/10.1016/j.jhydrol.2022.129006

FMI. ("n.d."). *Finska Meteorologiska Institutet - Öppen data*. https://sv.ilmatieteenlaitos.fi/oppen-data

Gascoin, S., Grizonnet, M., Bouchet, M., Salgues, G., & Hagolle, O. (2019). Theia Snow collection: high-resolution operational snow cover maps from Sentinel-2 and Landsat-

8 data. *Earth system science data*, *11*(2), 493-514. https://doi.org/10.5194/essd-11-493-2019

Hjort, J. (2006). *Environmental factors affecting the occurrence of periglacial landforms in Finnish Lapland: a numerical approach* University of Helsinki]. Aachen. https://www.researchgate.net/publication/47932730_Environmental_Factors_Affecting_the_Occurrence_of_Periglacial_Landforms_in_Finnish_Lapland_A_Numerical_Approach

Hori, M., Sugiura, K., Kobayashi, K., Aoki, T., Tanikawa, T., Kuchiki, K., Niwano, M., & Enomoto, H. (2017). A 38-year (1978–2015) Northern Hemisphere daily snow cover extent product derived using consistent objective criteria from satellite-borne optical sensors. *Remote Sensing of Environment*, *191*, 402-418. https://doi.org/10.1016/j.rse.2017.01.023

Hub, C. O. A. (2023). *Copernicus ESA Program*. Retrieved 23rd May from https://scihub.copernicus.eu/dhus/#/home

Keyser, S. R., Fink, D., Gudex-Cross, D., Radeloff, V. C., Pauli, J. N., & Zuckerberg, B. (2022). Snow cover dynamics: an overlooked yet important feature of winter bird occurrence and abundance across the United States. *Ecography*, *2023*(1). https://doi.org/10.1111/ecog.06378

Kinar, N. J., & Pomeroy, J. W. (2015). Measurement of the physical properties of the snowpack. *Reviews of Geophysics*, *53*(2), 481-544. https://doi.org/10.1002/2015rg000481

King, F., Kelly, R., & Fletcher, C. G. (2023). New opportunities for low-cost LiDAR-derived snow depth estimates from a consumer drone-mounted smartphone. *Cold Regions Science and Technology*, *207*. https://doi.org/10.1016/j.coldregions.2022.103757

Kopp, M., Tuo, Y., & Disse, M. (2019). Fully automated snow depth measurements from time-lapse images applying a convolutional neural network. *Sci Total Environ*, *697*, 134213. https://doi.org/10.1016/j.scitotenv.2019.134213

Korpilo, S., Virtanen, T., & Lehvävirta, S. (2017). Smartphone GPS tracking—Inexpensive and efficient data collection on recreational movement. *Landscape and Urban Planning*, *157*, 608-617. https://doi.org/10.1016/j.landurbplan.2016.08.005

Kujala, K., Seppälä, M., & Holappa, T. (2008). Physical properties of peat and palsa formation. *Cold Regions Science and Technology*, *52*(3), 408-414. https://doi.org/10.1016/j.coldregions.2007.08.002

Länsstyrelsen, N. (2014). *Kartering av Sveriges palsmyrar, Länstyrelsens rapportserie nr 4/2014.pdf>* (4/2014). https://www.lansstyrelsen.se/publikation?entry=_2014__7&context=31

Olvmo, M., Holmer, B., Thorsson, S., Reese, H., & Lindberg, F. (2020). Sub-arctic palsa degradation and the role of climatic drivers in the largest coherent palsa mire complex

in Sweden (Vissatvuopmi), 1955-2016. *Sci Rep*, *10*(1), 8937. https://doi.org/10.1038/s41598-020-65719-1

Proulx, H., Jacobs, J. M., Burakowski, E. A., Cho, E., Hunsaker, A. G., Sullivan, F. B., Palace, M., & Wagner, C. (2022). Comparison of in-situ snow depth measurements and impacts on validation of unpiloted aerial system lidar over a mixed-use temperate forest landscape. *The Cryosphere Discuss.*, *2022*, 1-20. https://doi.org/10.5194/tc-2022-7

Qfield. (2023). *QFIELD*. Retrieved 12 April from https://qfield.org/

Runge, A., & Grosse, G. (2019). Comparing Spectral Characteristics of Landsat-8 and Sentinel-2 Same-Day Data for Arctic-Boreal Regions. *Remote Sensing*, *11*(14). https://doi.org/10.3390/rs11141730

Sankey, T., Donager, J., McVay, J., & Sankey, J. B. (2017). UAV lidar and hyperspectral fusion for forest monitoring in the southwestern USA. *Remote Sensing of Environment*, *195*, 30-43. https://doi.org/10.1016/j.rse.2017.04.007

Sannel, A. B. K. (2020). Ground temperature and snow depth variability within a subarctic peat plateau landscape. *Permafrost and Periglacial Processes*, *31*(2), 255-263. https://doi.org/10.1002/ppp.2045

Sannel, A. B. K., Hugelius, G., Jansson, P., & Kuhry, P. (2016). Permafrost Warming in a Subarctic Peatland - Which Meteorological Controls are Most Important? *Permafrost and Periglacial Processes*, *27*(2), 177-188. https://doi.org/10.1002/ppp.1862

Seppälä. (2003). An experimental climate change study of the effect of increasing snow cover on active layer formation of a palsa, Finnish Lapland. *Proceedings of the 8th International Conference on Permafrost*, 1013-1016. https://doi.org/chrome-extension://efaidnbmnnnibpcajpcglclefindmkaj/https://www.arlis.org/docs/vol1/ICOP/55700698/Pdf/Chapter_177.pdf

Seppälä, M. (2006). Palsa mires in Finland. *The Finnish Environment*, *23*. https://www.researchgate.net/publication/266241369_Palsa_mires_in_Finland

Seppälä, M. (2017). Synthesis of studies of palsa formation underlining the importance of local environmental and physical characteristics. *Quaternary Research*, *75*(2), 366-370. https://doi.org/10.1016/j.yqres.2010.09.007

SMHI. (2022a). *Sveriges Meteorologiska och Hydrologiska Institut*. Retrieved 6 May from https://www.smhi.se/kunskapsbanken/klimat/jordens-klimat/jordens-huvudklimattyper-1.640

SMHI. (2022b). *Sveriges Meteorologiska och Hydrologiska Institut*. Retrieved May 6 from https://www.smhi.se/kunskapsbanken/klimat/sveriges-klimat/sveriges-klimat-1.6867

SMHI. ("n.d."). *Sveriges Meteorologiska och Hydrologiska Institut*. Retrieved April 14 from https://www.smhi.se/data

Verdonen, M., Störmer, A., Lotsari, E., Korpelainen, P., Burkhard, B., Colpaert, A., & Kumpula, T. (2023). Permafrost degradation at two monitored palsa mires in north-west Finland. *The Cryosphere*, *17*(5), 1803-1819. https://doi.org/10.5194/tc-17-1803-2023

Winsvold, S. H., Kaab, A., & Nuth, C. (2016). Regional Glacier Mapping Using Optical Satellite Data Time Series. *IEEE Journal of Selected Topics in Applied Earth Observations and Remote Sensing*, *9*(8), 3698-3711. https://doi.org/10.1109/jstars.2016.2527063

Žabota, B., Berger, F., & Kobal, M. (2023). The Potential of UAV-Acquired Photogrammetric and LiDAR-Point Clouds for Obtaining Rock Dimensions as Input Parameters for Modeling Rockfall Runout Zones. *Drones*, *7*(2). https://doi.org/10.3390/drones7020104

Zuidhoff, F. S. (2003). <*Palsa Growth and Decay in Northern Sweden pdf*> [Doctoral Dissertation, Uppsala University]. Uppsala, Sweden. https://www.diva-portal.org/smash/get/diva2:162423/FULLTEXT01.pdf

Zuidhoff, F. S., & Kolstrup, E. (2000). Changes in palsa distribution in relation to climate change in Laivadalen, northern Sweden, especially 1960-1997. *Permafrost and Periglacial Processes*, *11*(1), 55-69. https://doi.org/10.1002/(sici)1099-1530(200001/03)11:1<55::Aid-ppp338>3.0.Co;2-t

Appendix
Appendix A

Table A1. *Snow depth measurement points over the ridge-shaped & dome-shaped palsas.*

Snow depth points (cm) ridge-shaped & dome-shaped palsas			
Ridge in situ	Ridge LiDAR	Dome in situ	Dome LiDAR
55	48	70	32
40	74	0	0
51	4	0	0
35	59	45	18
45	55	32	48
60	53	55	12
0	53	50	83
0	8	60	45
0	35	80	50
46	61	52	65
60	36	48	51
55	44	0	14
0	9	35	52
0	37	0	13
0	10	32	150
0	54	52	49
0	7	73	54
0	9	145	29
39	19	0	14
77	35	0	14
41	26	46	65
49	47	40	46
42	56	77	56
0	18	28	54
52	11	58	46
0	0	50	48
0	12	52	43
60	20	40	29
33	76	0	17
0	6	0	23
35	36	0	37
0	10	66	13
26	34	70	116
64	33	53	40
90	19	41	41
66	44	68	28
90	74	20	45
30	18	72	58
51	24	49	53

Appendix B

Table B1. *Snow depth measurement points over the ridge-shaped & dome-shaped palsas.*

Snow depth points (cm) ridge-shaped & dome-shaped palsas			
Ridge in situ	Ridge LiDAR	Dome in situ	Dome LiDAR
52	26	39	54
15	49	23	31
0	14	16	22
0	13	51	62
0	4	50	62
63	66	0	16
0	6	37	23
0	3	64	12
52	143	87	94
56	63	61	30
90	83	61	45
46	93	74	86
97	77	53	16
88	88	30	15
56	52	0	15
59	65	34	21
53	71	26	10
0	9	0	10
0	12	110	104
0	4	45	77
0	28	49	71
55	0	70	57
98	16	48	58
0	1	68	142
0	104	102	83
0	6	105	100
34	98	59	44
95	76	62	26
119	21	79	24
25	15	57	20
50	16	66	42
78	26	67	47
120	90	99	45
40	15	117	79
115	131	0	12
100	165	119	149

Appendix C

Table C1. *Snow depth measurement points over the ridge-shaped palsa.*

Snow depth points (cm) ridge-shaped palsa	
Ridge in situ	Ridge LiDAR
98	110
20	0
38	37
118	136
130	182
30	0
12	3
75	39
135	122
45	61
20	37
38	58
50	69
71	71
56	58
0	6